Journal of Physics: Energy

PAPER

A brief introduction of electrode fabrication for proton exchange membrane water electrolyzers

Xinlong Lin[1,5], Justin Zhu Yeow Seow[1,2,5] and Zhichuan J Xu[1,2,3,4,*]

[1] School of Materials Science and Engineering, Nanyang Technological University, 50 Nanyang Avenue, Singapore 639798, Singapore
[2] Energy Research Institute@NTU (ERI@N), Interdisciplinary Graduate Programme, Nanyang Technological University, 50 Nanyang Avenue, Singapore 639798, Singapore
[3] The Cambridge Centre for Advanced Research and Education in Singapore, 1 CREATE Way, Singapore 138602, Singapore
[4] Center for Advanced Catalysis Science and Technology, Nanyang Technological University, 50 Nanyang Avenue, Singapore 639798, Singapore
[5] These authors contributed equally to this work.
[*] Author to whom any correspondence should be addressed.

E-mail: xuzc@ntu.edu.sg

Keywords: water electrolysis, membrane electrode assembly, proton exchange membrane, electrocatalysts, electrodes, hydrogen

OPEN ACCESS

RECEIVED
7 December 2022

REVISED
16 March 2023

ACCEPTED FOR PUBLICATION
13 April 2023

PUBLISHED
5 May 2023

Abstract

Proton exchange membrane water electrolyzer (PEMWE) is a major enabler of green hydrogen production. The development of water electrolyzers is a vital step in driving the progress of a hydrogen-based economy. The system inside the electrolyzer is a zero-gap cell featuring low ohmic resistance and boosted mass transport, leading to higher energy efficiency and minimized capital cost. Besides, utilizing PEM in the electrolyzer for sustainable hydrogen production enables the system to perform with many advantages, including superior energy efficiency, higher hydrogen purity, and high flexibility. Therefore, as PEM electrolyzers continue to evolve, sustainable hydrogen production on a larger scale will be realized in the near future. This review summarizes the status quo of PEM water electrolyzers in the past four years. We will start with a brief introduction of the core of a water electrolyzer, namely the membrane electrode assembly (MEA), which will be followed by an introduction of fabrication methods of MEA, including CCM methods, catalyst-coated electrode methods, and other innovative fabrication methods. Next, we will summarize recent attempts to modify electrodes and membranes in MEAs to promote the performance of PEMWE. Subsequently, catalyst development for hydrogen evolution reaction (HER) and oxygen evolution reaction (OER) in MEA is discussed, highlighting novel HER/OER catalysts and strategies to reduce the content of noble metals. Lastly, conclusion and perspectives are provided to present a blueprint to inspire the future development of PEMWE.

1. Introduction

In response to the increasingly urgent need for energy sustainability and growing environmental problems, significant amount of resources has been allocated to the research and development of renewable energy storage and conversion. Hydrogen, a promising clean fuel with a high specific energy (140 MJ kg^{-1}), has an important role in achieving carbon neutrality envisioned by the international community. Thus, particular attention has been paid to replace conventional hydrogen production via steam methane reforming (SMR) at high temperature and under high pressure that emits flue gas with a carbon-free alternative.

Hydrogen production from water splitting powered by electricity has emerged as a prospective alternative to the fossil-fuels-based technology that enables hydrogen synthesis in milder conditions without producing environmentally detrimental by-products [1]. The two half-reactions in the electrochemical water splitting (or water electrolysis) are the cathodic hydrogen evolution reaction (HER) and the anodic oxygen evolution reaction (OER). The currently well-known set-ups for water electrolysis include solid oxide electrolysis cell, polymer electrolyte membrane electrolysis cell (PEMEC), anion exchange membrane electrolysis cell, and alkaline electrolysis cell [2, 3], the most prominent of which is PEMEC as its life cycle assessment, when

powered by renewable energy sources, has demonstrated its potential in substantially reducing CO_2 emission of hydrogen production when it replaces SMR [4]. While efficiency of water electrolysis (around 60%–80%) can be comparable to that of SMR (65%–75%) [5], it only accounts for 4% of global hydrogen supply, mainly for yielding high-purity oxygen and small-scale hydrogen production [6–9], due to its high cost and limited efficiency, the joint result of which renders this technology less competitive in the current market.

Water electrolyzers with proton exchange membrane (PEM) is the most prominent technology for sustainable hydrogen production in an acidic environment. Compared with a cheaper and established alkaline water electrolyzer (AWE) technology, PEM water electrolyzer (PEMWE) has current density at rated full-power of between 1 and 3 A cm^{-2}, which is almost four times higher than that of AWE (<0.5 A cm^{-2}) [10, 11]. Besides, it outperforms in other aspects such as energy efficiency (up to 95%), hydrogen purity (99.99%), ability to manage fluctuating power input, versatility of operating temperature range, ability to reduce gas crossover, thermal and chemical stability, lifetime, and direct utilization of pure water as feedstock [12–14]. The acidic environment created by PEM improves HER through the direct utilization of protons to generate pure hydrogen while avoiding unfavorable formation of carbonate contaminants that readily occur in the alkaline environment [15, 16].

The primary factor to be considered in maximizing the hydrogen production efficiency in PEMWE is the choice of electrocatalysts. The benchmark electrode materials for PEMWE in corrosive acidic environment comprise of mainly noble metals, such as IrO_2, RuO_2 and Pt, whereby Pt is preferred for catalyzing HER while IrO_2 and RuO_2 possess the best performance for OER [17, 18]. Despite the impressive performance, their scarcity and high cost call for developing electrocatalysts with higher performance and cost efficiency. Moreover, although the leading reaction for hydrogen production is HER at the cathode, kinetic limitation originating from OER at the anode imposes a barrier in the water electrolysis since it involves a sluggish transfer of four electrons while HER only needs to transfer two electrons [19]. Although the theoretical thermodynamic potential for overall water splitting (OWS) is 1.23 V, additional energy is required to overcome the reaction barrier of the OWS, a major fraction of which is associated with the losses in OER, thereby requiring a larger voltage in the practical electrolysis [20]. In other words, OER governs the overall efficiency of water electrolyzers.

Besides, the advancement of PEMWE is supported by device-level electrolyzer development, which is chiefly dependent on that of its smallest electrolysis cell unit, namely membrane electrode assembly (MEA). Compared with the conventional planar electrode and aqueous gas diffusion electrode, MEA is a zero-gap cell with low ohmic resistance and boosted mass transport, thus leading to higher energy efficiency at minimum cost [21–23]. Nonetheless, its widespread commercialization requires further improvement in performance, cost and lifetime [24]. The sandwich-structured MEA (figure 1) typically consists of a membrane as well as a catalyst layer (CL) and a gas diffusion layer (GDL) on each of cathodic and anodic substrates [25]. Additionally, its hardware includes bipolar plates containing flow fields inside to channel the flow and gaskets enabling a gas-tight seal of the MEA. Its catalytic efficiency depends on the formation of triple-phase boundaries (TPBs) between the electrolyte, the electrocatalyst, and the gaseous product with reduced resistance of mass transfer and charge transfer [26, 27]. Therein, besides facilitating mass transport of the products, GDL is also expected to conduct the electrons from the CL to bipolar plates and provide mechanical support for the membrane [28, 29]. When the GDL is coated with a microporous layer to form a porous transport layer (PTL), a flat and uniform layer between the CL and the carbon substrate is formed to further reduce the contact resistance and to act as a layer to balance between water retention and water removal abilities, thus boosting the cell performance [30–33]. In PEMWE, a carbon substrate is usually used for the cathode PTL, while the PTL consisting of titanium is typically applied at the anode side of the electrolyzer owing to its highly corrosive environment. Due to the advantageous configuration of MEA, the use of MEA as a tool to study the performance of electrocatalysts is gaining attention [34–38].

Herein, the status quo of PEMWE MEA during the past four years is reviewed, starting from an introduction of the fabrication methods of catalyst-coated components in MEA, including catalyst-coated membrane (CCM), catalyst-coated electrode (CCE), and other fabrication methods. Next, we will cast a view on the emerging modification strategies on electrodes and membranes to ameliorate the performance of PEMWE. Subsequently, catalyst development for HER and OER in MEA is discussed, highlighting the novel catalysts and strategies for reducing the loading of precious metals. Finally, conclusions and perspectives are proposed to inform the development of next-generation water electrolyzers.

2. Fabrication of catalyst-coated components

While reduction of charge transfer and mass transport resistances in PEMWE can be improved through improvement of contact between components and effective design of manifolds, its efficiency is still mainly

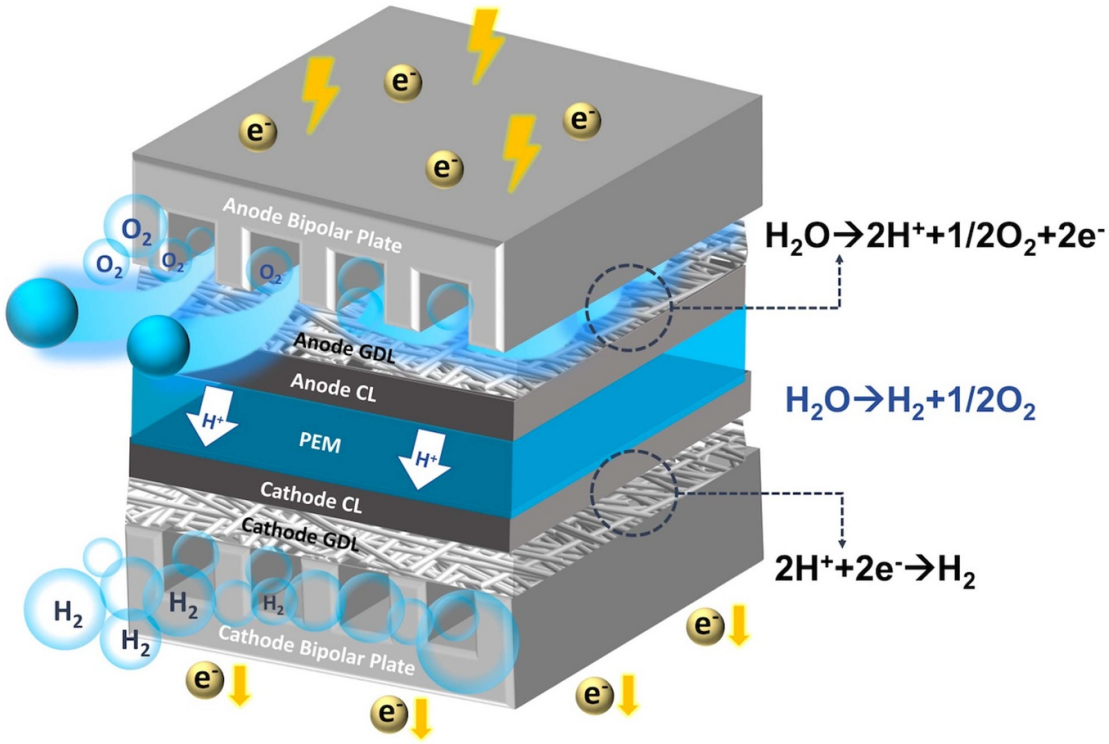

Figure 1. Graphical illustration of a MEA and the electrochemical reactions occurring at the catalyst layers.

limited by the reaction kinetics at the electrode. Hence, the incorporation of electrocatalysts in PEMWE is vital. By and large, there are two common categories of methods of incorporating electrocatalysts, namely, CCE and CCM. The former is the most robust preparation strategy involving coating catalyst on the surface of GDLs using brush or spray coating and the latter is more exclusively used to deposit two CLs on both sides of the membrane, either directly via spray coating or indirectly by transferring the catalyst to the membrane surface through a decal process [28]. In this section, common MEA fabrication strategies for PEMWE, followed by some innovative approaches, will be introduced to serve as a cornerstone for further discussion on the performance of MEA for hydrogen production.

2.1. Catalyst-coated electrode (CCE)

In general, the CCE methods can achieve a better intermediary contact between the CL and PTL. Although they are still underdeveloped for scaling up and preferable for MEA size smaller than 50 cm^2, they have been demonstrated to have less catalyst loss compared to the CCM methods [28]. The general procedure of preparing a CCE (also known as gas diffusion electrode, GDE) is shown in figure 2(a), where the catalyst ink with ionomer is coated on the surface of GDL either by brush or by spray, followed by drying to obtain a CCE, in which the ionomer serves as an adhesive between the GDL and the membrane while creating pathways for proton transportation from the TPB to the electrolyte [28]. The catalyst-coated GDL is then hot-pressed to the membrane to manufacture MEA. This step is crucial as weak catalyst-membrane interaction is the main cause of poor performance in CCE-MEA.

The combination of the thin ionomer overlayer and hot pressing of the CCE to the membrane is important for fabricating a MEA with performance that can match those of CCM-MEAs [39]. The overlayer smoothens the GDE surface and improves the adherence of GDE to the membrane, providing more intimate contact between the CL and the membrane, thereby reducing ohmic losses and increasing catalyst utilization. Apart from that, there are other emerging ways of engineering catalyst-membrane interface either from the CL side by (1) using graded or patterned CLs and (2) forming ionomer-impregnated catalyst surfaces, or from the membrane side by (1) direct deposition of membrane, (2) fabricating patterned membrane, and (3) forming porous membrane surface [40].

The performance of GDE can be further improved by tuning the catalyst thickness to surpass the performance of CCM-MEA as demonstrated by Kang *et al* through *in-situ* visualization of the hydrogen evolution in different PEMWE cells [41]. In this study, a novel thin GDE with a CL thickness of 15 $\sim$ 90 nm and a 25 μm thin and tunable liquid/GDL (TT-LGDL) was prepared and compared with the conventional

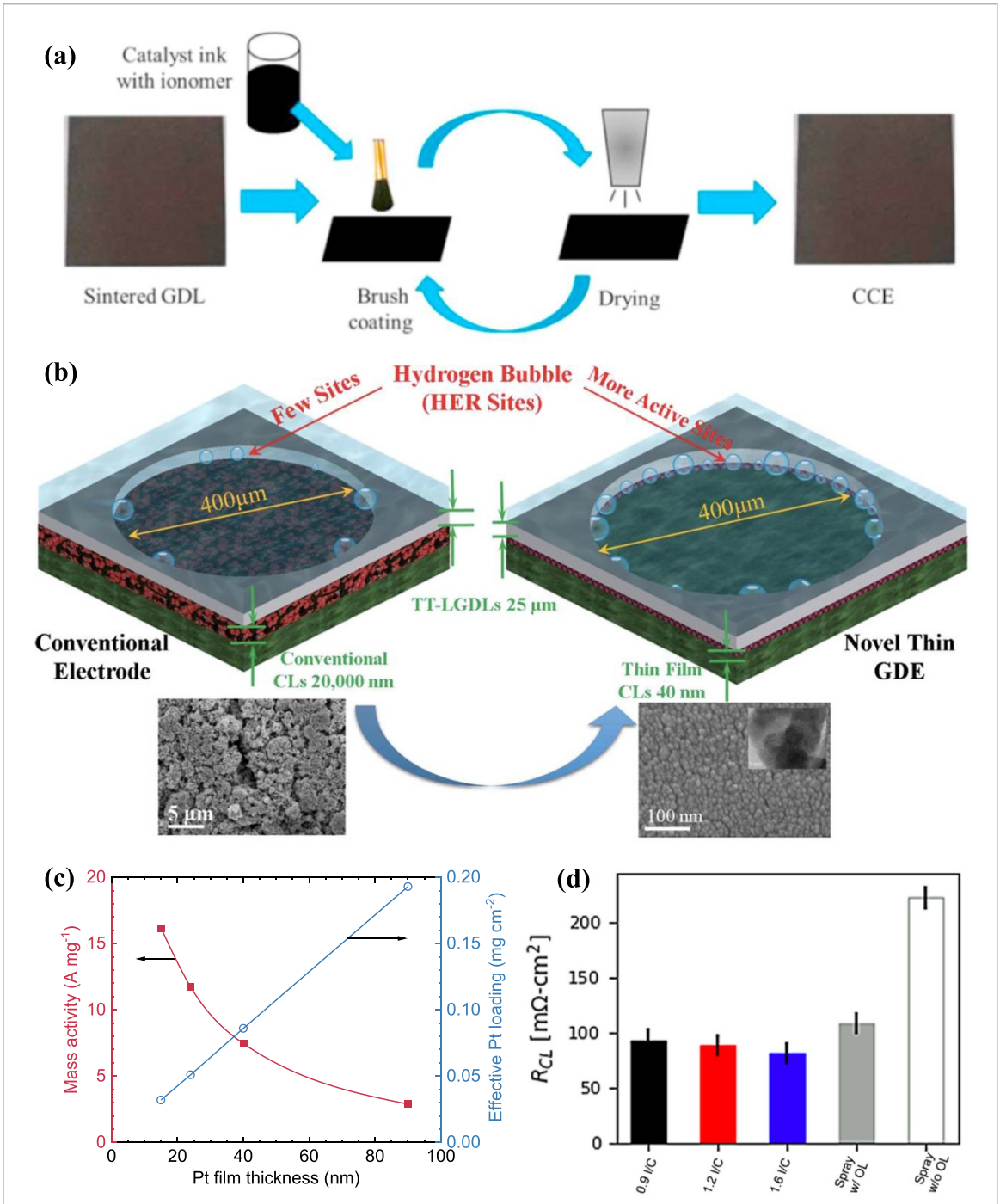

Figure 2. (a) Schematic diagram of MEA fabrication via CCE using the brush coating method. Reprinted from [28], Copyright (2020), with permission from Elsevier. (b) *In-situ* visualization of hydrogen evolution reaction in the conventional CCM-based electrode and novel thin GDE. Reprinted from [41], Copyright (2018), with permission from Elsevier. (c) Plots of mass activity at 1.6 V and effective Pt loading versus Pt film thickness on TT-LGDLs based on data from [41]. (d) R_{CL} values of R2R-coated GDEs with different I/C ratios and spray-coated GDE with (w/OL) and without overlayer (w/o OL). Reprinted from [45], Copyright (2021), with permission from Elsevier.

electrolyzer fabricated using CCM. In figure 2(b), the novel thin GDE exhibited more HER active sites compared to the thicker conventional CLs in conventional CCM set-up due to the larger electrical resistance caused by the lack of uniformity of catalyst distribution in the latter. With novel thin GDE at ultra-low catalyst loading, catalyst utilization and Pt catalyst mass activity increased, resulting in more hydrogen bubble generation occurring at the rim of the observation hole. At low CL thickness of 15 nm and low effective Pt loading of 0.032 mg cm^{-2}, its mass activity could reach as high as 58 times that of the conventional CCM at 1.6 V, 80 °C and 1 atm (figure 2(c)).

To date, many techniques are available to manufacture GDE [42, 43], and hence, an effective comparison between them is essential in providing meaningful insights for further improvement in GDE fabrication. A

recent study has made a comparison between CCM by dry spraying and GDEs by airbrush, screen printing, doctor blade, drop casting, and inkjet printing to investigate the difference in CL microstructures, mass transfers and charge transfers [44]. In the study, ionomer coverage on Pt/C decreased in the following order: airbrush > screen printing > dry spraying > drop casting > inkjet printing > doctor blade. This result was consistent with the higher electrochemically (EC) active surface area (ECSA) values of GDEs fabricated by airbrush and screen printing, demonstrating higher catalyst utilization at higher ionomer coverage. Upon considering charge and mass transport properties, the three best MEAs were obtained by airbrush, screen printing and ink jet methods as they showed optimal balance of properties such as ohmic resistance, porosity, and covered Pt. Particularly, GDE fabricated by screen printing exhibited a high fraction of ionomer covered Pt/C and good charge and mass transport properties, delivering the best performance at high currents.

To enable the mass production of MEAs, a continuous production process is needed. Considering the relatively robust mechanical properties of the diffusion media and the low tendency of membrane swelling during CL coating, Mauger *et al* applied the continuous roll-to-roll (R2R) process in CCE-MEA manufacturing, where the CL was coated using a slot die with a slot gap of 250 μm and a coating width of 8 cm, followed by drying at 80 °C in the air flotation ovens in the coating line [45]. By adjusting the ionomer-to-carbon ratio (I/C) in the coating ink and drying parameters, a CL with an ionomer-rich top surface was prepared, eliminating the ionomer overlayer that is typical in spray-coated GDEs and reducing the production cost. Moreover, the protonic sheet resistance of the CL (R_{CL}, consisting of the bulk CL resistance and the catalyst-membrane interfacial resistance) of R2R-coated GDEs were lower than that of spray-coated GDEs with an ionomer overlayer. While a slight decrease in R_{CL} with increasing I/C ratio was observed (figure 2(d)) resulting from the increased proton conductivity, the decreased resistance did not improve their performance significantly, possibly due to the excessive filling of the catalytic pore space and hence, 0.9 I/C was considered optimal in forming a good interface while preventing inhibition of gas diffusivity.

2.2. Catalyst-coated membrane (CCM)

Coating the CLs on the membrane is conducive for close contact between the catalyst and electrolyte membrane to form a strong interfacial connection, which usually improves MEA performance while reducing catalyst loading [46, 47]. Hence, a CCM is usually used to fabricate a MEA that outperforms CCE-MEAs owing to its low contact resistance [48]. In a comparative study, Moghaddam and Easton fabricated both CCM-MEA and CCE-MEA by spray coating and demonstrated that CCM-MEA generally outperformed CCE-MEA in fuel cells owing to the more coherent surface structure and lower charge transfer resistance [49]. Similarly, Bühler *et al* showed that CCM-MEA had better kinetics than the CCE-MEA in the PEM water electrolysis despite exhibiting an inferior polarization behavior and inferior performance reproducibility to CCE-MEA for current densities above 750 mA cm^{-2} [50].

Notwithstanding the possibility of direct coating of a membrane, the decal process, involving an indirect transfer of CL to the membrane, is the representative coating approach for CCM that is most suited for MEA mass production in the manner shown in figure 3(a). The catalyst ink is first prepared by mixing the catalyst, an ionomer, and suitable solvents, followed by coating the ink mixture on the decal substrate (e.g. Kapton film or Teflon film) using a doctor blade to spread the ink uniformly on the substrate [51]. After drying (which can affect the formation of effective three-phase boundary during operation), the CL is cut and sent for hot-pressing to tighten the adhesion of the anode, the cathode, and the membrane. In the end, the decal substrate is peeled off from the electrodes. Despite being the most favorable for mass production, several shortcomings of this process need to be resolved, namely [51, 52]: (1) mitigating the incomplete transfer of the catalyst to the membrane; (2) optimizing the temperature and pressure during hot-pressing as the ionomer and membrane may not withstand high temperatures; (3) delicate design of the catalyst ink with suitable composition to improve catalyst utilization; and (4) engineering the microstructure of the CL to expedite the transport of the gaseous product during electrolysis.

The property of the decal substrate is the crux for an efficient transfer of the CL; thus its material selection is important. From a study involving polypropylene (PP), low-density polyethylene, silicone coated polyethylene terephthalate, polytetrafluoroethylene (PTFE), reinforced-PTFE, and Kapton films, Akella *et al* implied that PP is the most suitable material for decal substrates [53]. PP was shown to possess superior thermal stability during hot-pressing and higher hydrophobicity that checked the coagulation of the catalyst ink slurry cast. Importantly, 100% catalyst transfer to the Nafion membrane was observed with PP.

Low-temperature decal transfer was also developed to further reduce the cost of the decal process and further enhance the MEA performance by tuning of properties of the membrane material. For example, Kyeong *et al* synthesized new aliphatic backbone-containing sulfonated poly (arylene ether sulfone)s (HexX), which was suitable for fabricating MEAs via low-temperature decal transfer [54]. Introducing the hexyl groups between biphenyls improved the flexibility of the backbone, which reduced the glass transition

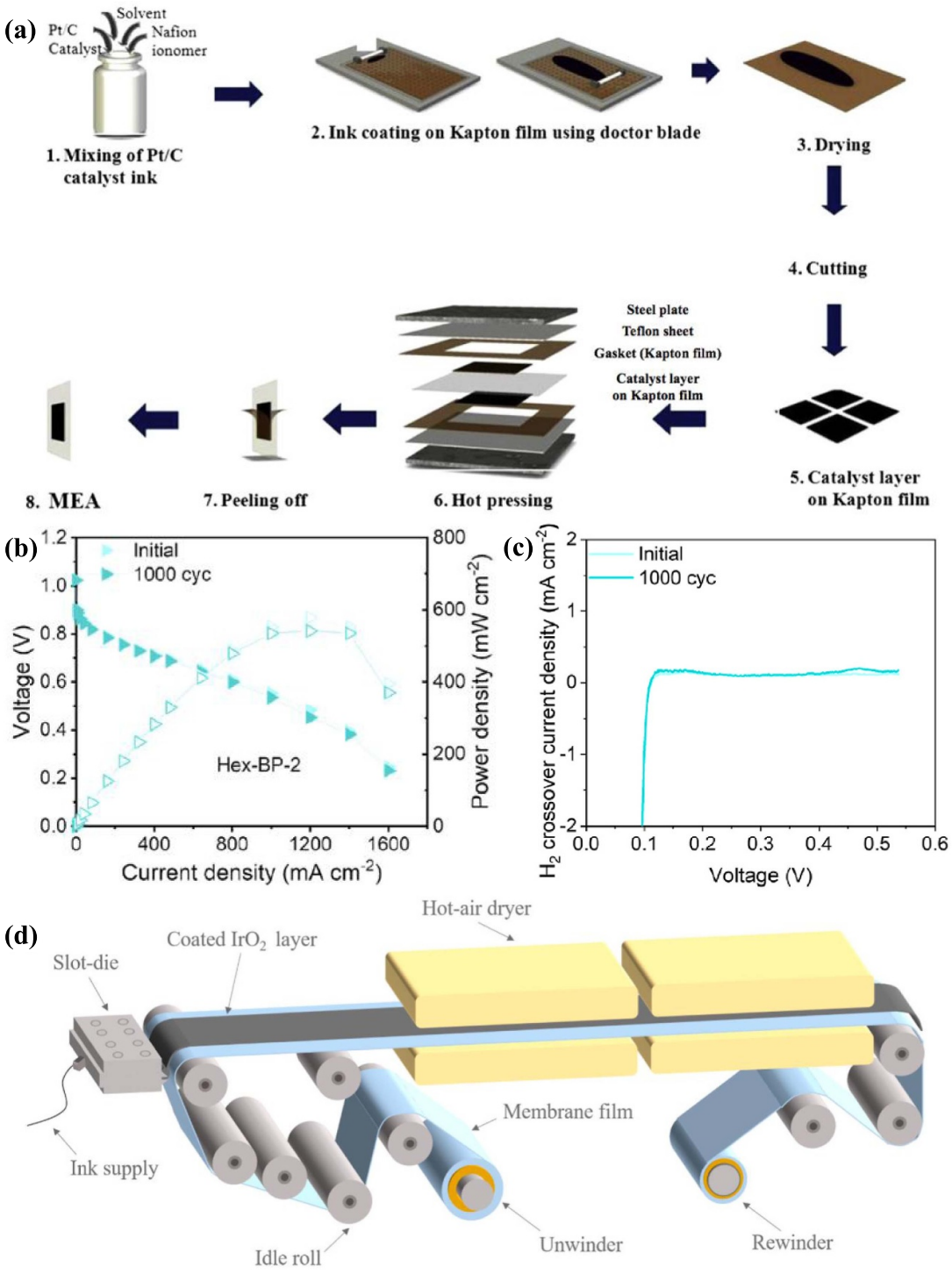

Figure 3. (a) Schematic diagram of MEA fabrication via a decal process. Reprinted from [51], Copyright (2011), with permission from Elsevier. (b) Single-cell performance of Hex-BP-2 in 1000 cycles of the wet-dry cycling test and (c) linear sweep voltammetry (LSV) curves of Hex-BP-2 before and after 1000 cycles of the wet-dry cycling test. Reprinted from [54], Copyright (2022), with permission from Elsevier. (d) Schematic diagram of large-scale R2R catalyst coating. Reprinted from [55], Copyright (2020), with permission from Elsevier.

temperature (T_g) of the membrane, facilitating the easy transfer of the CL from the substrate to the membrane due to the rubber-like state of the polymer near T_g. With further blending of HexX with biphenyl-containing sulfonated poly (arylene ether sulfone)s (BPSXs) to form a blend membrane (Hex-BP), the stability of MEA fabricated from Hex-BP-2 (consisting of 50.93 mol% Hex and 49.07 mol% BP) was greatly enhanced to withstand over 1000 wet-dry cycles (figure 3(b)). Besides, low H_2 crossover current densities of 0.12 and 0.13 mA cm^{-2} were maintained for Hex-BP-2 before and after 1000 wet-dry cycles respectively (figure 3(c)).

Although membrane swelling is effectively eliminated by direct application of a dry CL on the membrane, an additional step of transferring CL from the decal substrate to a membrane is required, which is not desirable for mass production. To this end, the use of a R2R process for large-scale CCM-MEA fabrication was studied by Park *et al* to replace the decal process [55]. A large-area PEMWE MEA is produced by directly coating the IrO_2 catalyst on the membrane through a R2R process, where sheets of membrane film were spliced to create a long web to cover the path of the R2R system and a slot die was used for continuous coating process, followed by in-line drying in the hot-air dryer (figure 3(d)). The production throughput was increased by over 500 times at a low temperature in contrast with the laboratory-scale spray coating. The performance of the resultant water electrolyzer is also comparable to that with spray-coated CCMs, with a cell voltage of 1.91 V at a current density of 2 A cm^{-2}.

2.3. Other fabrication methods

The common MEA fabrication methods show the tremendous potential in the current development of MEA manufacturing. Notably, MEAs prepared by the CCM methods have lower interfacial resistance between the membrane and CL than those prepared by the CCE methods, but CCMs can easily form cracks in the CL due to the vaporization of the solvent in the catalyst ink as well as the swelling of the membrane [56, 57]. In view of the limitation of traditional methods, novel MEA fabrication methods are desired to overcome these challenges.

Notably, the direct membrane deposition (DMD) is first proposed by Klingele *et al* for fuel cell preparation, in which dispersed polymer electrolyte was directly deposited on the CLs of the anodic and cathodic electrodes [58]. Stähler *et al* first applied the DMD method in fabricating PEMWE MEA, where the cathodic CL, a membrane with 20 ± 2 μm, and the anodic CL were successively slot-die-coated layer by layer on each other [59]. This allowed free selection of the PTL in the MEA, and simultaneously, the formation, properties, and composition of each layer can be controlled. As a result, the reduced interfacial resistance was ascribed to good contact between different layers. However, the thinness of the membrane and the quick corrosion of carbon are set to challenge industrial operation of this PEMWE MEA.

To further improve the DMD approach, Holzapfel *et al* prepared DMD-MEA with a titanium substrate at the anode side and suitable membrane thicknesses of 60 μm, 200 μm, and 230 μm for realistic operation, in which the membrane was asymmetrically deposited solely on the cathodic substrate instead of using the symmetric DMD design (figure 4(a)) [60]. In this method, PTFE frames were used to center the MEA and the configuration is shown in figure 4(b). When compared with CCM and porous transport electrode (PTE)-type MEAs, DMD-MEA exhibited improvement in the electrochemical performance (figure 4(c)), with membrane thickness of 60 μ m being ideal owing to the reduced kinetic, ohmic, and mass transport losses.

However, in the conventional DMD process, the catalyst particles can fill the pores of microporous layers during catalyst coating in GDE fabrication, which will influence the surface morphology of the CL, further affecting the polymer morphology after dispersing the ionomer on GDE. A novel approach was then proposed by Yang *et al*, where Nafion ionomers were directly coated on both cathode and anode CLs, followed by hot pressing of both ionomer-coated CLs and attaching GDLs on both CLs [61]. In this MEA, crack formation on the CL surface was mitigated (figure 4(d)). Besides, expanded PTFE (ePTFE) film was attached on the ionomer layer of ionomer-coated cathodic CL before hot pressing with the ionomer-coated anodic CL to provide meliorative mechanical properties and stability of the resultant MEA. This enhancement was verified by Xing *et al* when ePTFE was added to one of the ionomer-coated GDEs (figure 4(e)) [57]. In addition, Shang *et al* impregnated a porous ePTFE matrix with crosslinkable poly (phenylenesulfonic acid) (cPPSA) to form a composite cPPSA-ePTFE membrane, enhancing the proton conductivity of the membrane [62]. The thickness of the ePTFE-reinforced membrane deposited on the electrode will be a vital consideration in future research to reduce interfacial resistance.

CCM and CCE methods are still two dominating classes of fabrication methods for MEA production in mainstream studies despite the tremendous endeavors made in enhancing these approaches and even replacing them. By exploring the main contributors to the elevated performance brought by various innovations and working towards fully addressing the thorny challenges in both material synthesis and device fabrication in the industrial setting, more opportunities to upscale MEA fabrication can be created.

3. Electrode and membrane modifications

The fabrication procedure of the MEA is influential to the performance of water electrolysis. By delicate design of the fabrication procedures, researchers emphasize more on maximizing the contact area between different layers and finding ways to promote mass and charge transfer by tuning interlayer interactions. However, electrodes and membranes can be creatively modified to further optimize the property of MEAs for

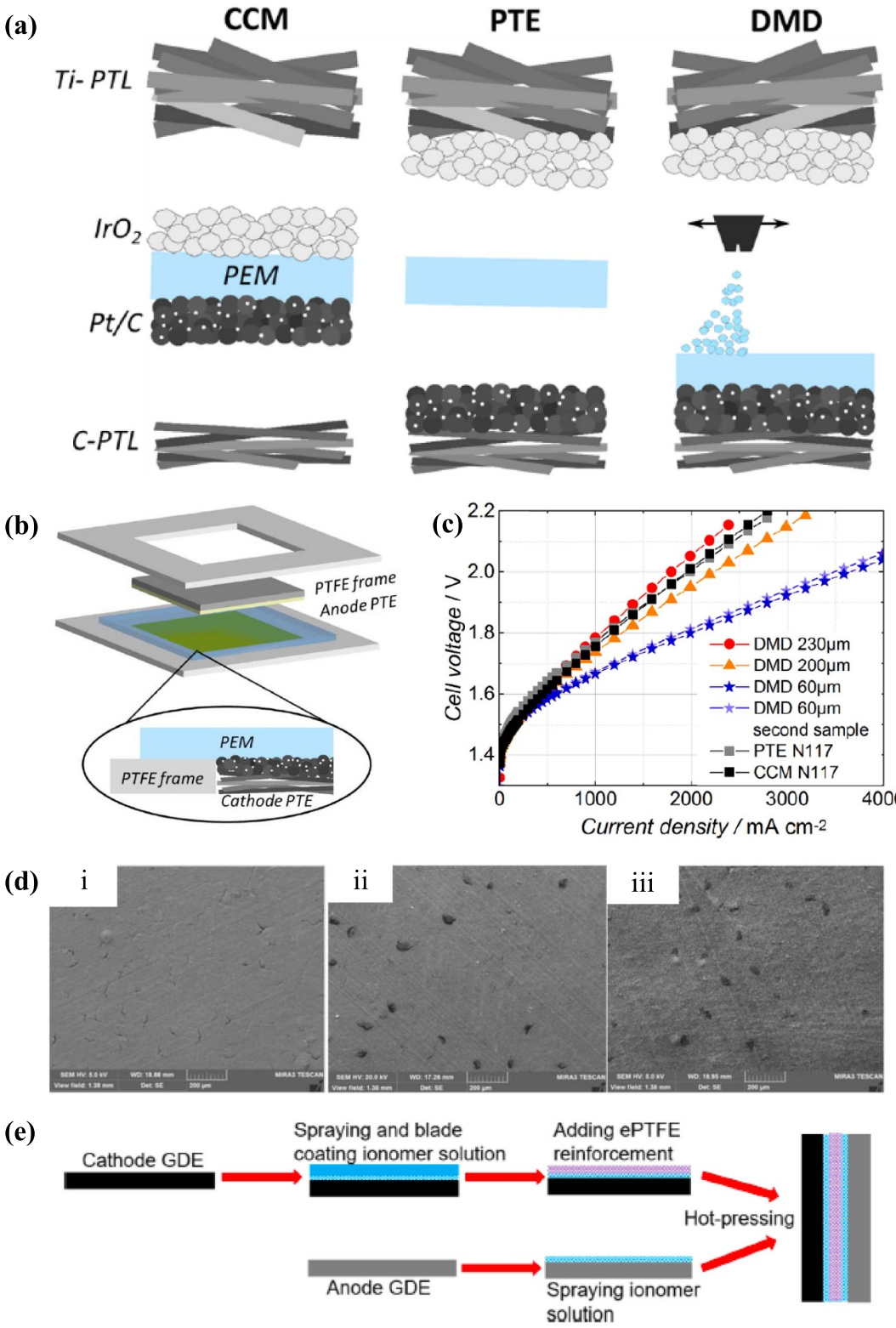

Figure 4. (a) A schematic comparison of MEA fabrication through a CCM method (left), establishing porous transport electrode (PTE) (center), and DMD via spray coating (right), (b) schematic illustration of the novel DMD-MEA configuration, and (c) polarization curves of DMD-MEAs with various membrane thicknesses and reference samples (PTE using Nafion 117 membrane and CCM using Nafion 117 membrane). Reproduced from [60]. CC BY 4.0. (d) SEM images of the top surface of the catalyst layer for (i) conventional decal-transferred MEA (C-MEA), (ii) novel MEA (N-MEA), and (iii) novel ePTFE reinforced MEA (N-R-MEA). Reprinted with permission from [61]. Copyright (2020) American Chemical Society. (e) Schematic illustration of fabrication of reinforced MEA by combining the ePTFE and DMD approaches. Reprinted with permission from [57]. Copyright (2022) American Chemical Society.

efficient water electrolysis. In this section, modification strategies that have been employed on electrode and membrane to ameliorate the PEMWE performance during recent years will be reviewed and discussed.

3.1. Electrode modification

Modifying the morphology of the electrode can help to establish an efficient charge transport pathway and reduce the loading of catalysts. For instance, by changing the morphology to a 1D nanostructure, a large aspect ratio of the nanostructure facilitated the improvement of electric conductivity [63]. Xie *et al* fabricated an integrated HER electrode design comprising *in-situ* grown Pt nanowires (PtNWs) on the thin Ti LGDLs (TT-LGDLs), which was chemically synthesized on Ti substrates via a surfactant-free process [64]. Compared with the conventional GDE (figure 5(a)), the electrode thickness was successfully reduced from $\sim$300 μm to $\sim$25 μm, and the application of PtNW GDE improved the catalyst utilization by exposing more catalyst surface to contact with electrolyte to increase the concentration of TPBs. The smooth LGDL surface was completely covered by a CL with a small loading of 0.045 mg cm^{-2} and this morphology was maintained after a stability test of 10 h at 100 mA cm^{-2}. Moreover, a faster gas bubble removal rate was observed in PtNM/Ti electrode due to the increased surface roughness, thus reducing bubble coverage. As a result, this electrode with catalyst loading of 0.2 mg_{Pt} cm^{-2} reached the lowest cell voltage of 1.643 V and high cell efficiency of 90.08% at 1 A cm^{-2} in the PEM electrolyzer cell. A similar morphology modification strategy was employed by Kang *et al*, in which a novel 2D-patterned electrode (figure 5(b)) exhibited boosted catalyst utilization and mass activity [65]. This 2D-pattern electrode consisting of CL stripes (with the optimal set-up comprising 1.0 mm catalyst stripes and 0.3 mm gap) was synthesized using a shadow mask on the Nafion membrane, followed by spraying of the catalyst ink. In this system, the edge effect on the anode was induced by the membrane property, proton conduction path, internal potential distribution, and catalytic sites distribution to assist the transport of generated protons in OER to a further region to reach the cathode HER active sites. The optimal 2D-pattern electrode saved more than 21% of the anodic noble metal material while maintaining the same performance of the system where the anode fully covered the membrane.

As mentioned, OER will restrict the OWS owing to its sluggish kinetics. In the meantime, the co-production of hydrogen and oxygen as well as the use of PEM restrict the direct utilization of sporadic and fluctuating renewable energy, causing the formation of a hazardous H_2/O_2 mixture [66]. Although PEM is required to prevent gas crossover, its high cost is the main consideration, and hence, finding a way to decouple the OER and HER becomes significant, through which even the use of membrane can be eliminated. To this end, several solid-state redox mediators have been reported up to now, such as pyrene-4,5,9,10-tetraone [67], polyaniline [68], nickel hydroxide [69], and polytriphenylamine [70]. By incorporating them as auxiliary electrodes, the ion exchange between the anode and cathode is mediated, enabling the production of hydrogen and oxygen at different time and space [71]. For example, Liang *et al* create an innovative and low-cost hydrated Turnbull's blue analog (TBA) electrode, which served as a solid-state redox mediator (figure 5(c)) [66]. The CuFe-TBA was synthesized by a facile co-precipitation method. There were two steps in the decoupled water electrolysis, the first of which involve oxygen production and cathodic CuFe-TBA reduction, followed by hydrogen production associated with the anodic oxidation of reduced CuFe-TBA. As a result, the redox mediator showed a reversible capacity of 80 mAh g^{-1} at a current density of 0.5 A g^{-1} and achieved high-rate performance with a respectable capacity of 42.7 mAh g^{-1} at a high current density of 120 A g^{-1} (figure 5(d)). They fabricated a PEM-less electrolyzer assembled from a Pt-coated Ti mesh electrode, a RuO_2/IrO_2-coated Ti mesh electrode, and a CuFe-TBA film electrode, which was investigated in 0.5 M H_2SO_4 by chronopotentiometry. The OER process gave an average cell voltage of around 0.68 V at an applied current of 5 mA for step 1, while step 2 exhibited a cell voltage of 0.9 V, summing up to obtain an overall voltage of 1.58 V (figure 5(e)). Moreover, the cell voltage of step 1 and step 2 remained stable after a 170 h cycling test, indicating the superior durability of this novel electrode.

Since OER kinetics is the main obstructor in water electrolysis, improving mass transport and cost efficiency in the PTLs on the anode is thus indispensable in removing the barrier to better MEA performance. By varying the thickness and porosity of fiber-sintered titanium PTL on the anode, Peng *et al* studied the impact of bulk and interface transport properties of PTLs on PEMWE performance at ultra-low Ir loading (0.05 mg_{Ir} cm^{-2}) [72]. They demonstrated that the optimal kinetics was reached in the PTLs with intermediate porosity and interfacial area due to the balance between oxygen removal and water accessibility, reducing the resistance for electrons to transport through the interface. Besides, the mass transport resistance (or overpotential) can be reduced by increasing PTL porosity and reducing through-plane tortuosity. Furthermore, the influence of PTL in different forms was studied by Bühler *et al*, where the anodic porous

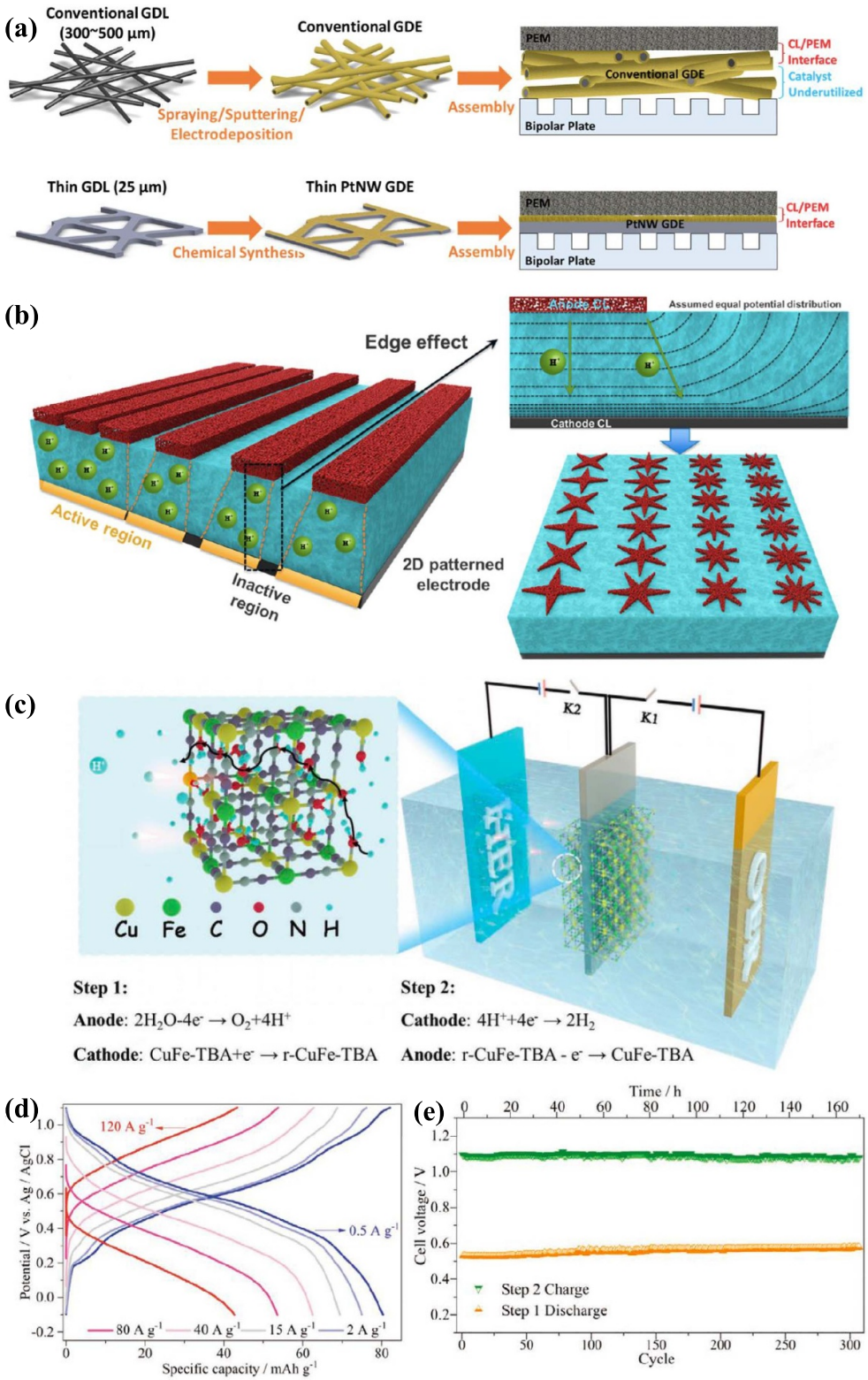

Figure 5. (a) Graphic comparison between novel GDE with *in-situ* grown Pt nanowires and conventional GDE. Reprinted from [64], Copyright (2020), with permission from Elsevier. (b) Schematic illustration of CCMs with a 2D-patterned electrode (left) and working mechanism of edge effect as well as the future generation of a 2D patterned electrode (right). Reprinted with permission from [65]. Copyright (2022) American Chemical Society. (c) Schematic illustration of decoupling water electrolysis using CuFe-TBA as a solid-state redox mediator, (d) charge/discharge curves at different current densities for decoupling water electrolysis and (e) the stability test of the CuFe-TBA electrode at 10 mA with a step time of 1000 s for decoupling H_2 and O_2 production from water electrolysis. [66] John Wiley & Sons. © 2021 Wiley-VCH GmbH.

fiber-sintered PTL outperformed the powder-sintered one for loading above 1.0 mg_{IrO2} cm^{-2} owing to lower ohmic loss [73].

In developing modified PTLs, Stiber *et al* produced novel PTLs by diffusion bonding of a Ti porous sintered layer (PSL) on a Ti expanded metal mesh (PSL/mesh-PTL), which eliminated the use of flow field in the bipolar plates [74]. The PSL that possessed a uniform pore size distribution was fully bonded to the mesh-PTL. This new PTL allowed efficient gas/water management at high current densities. The high liquid and gas permeability contributed to ameliorated performance at a high current density of 6 A cm^{-2} under extreme conditions of either 90 °C or 90 bar H_2 output. At a nominal load of 4 A cm^{-2}, higher efficiency was also observed for PSL/mesh-PTL compared to the common mesh-PTL that exhibited significant energy loss due to mass transport.

Owing to the corrosive environment at the anode, the PTL typically consists of titanium at the anode. However, the protective passive layer covered on the Ti surface (oxide/hydroxide) leads to high surface contact resistance originating from its lack of electrical conductivity [75, 76]. This results in loss of energy, which is exacerbated during the intensive operation at large current densities [77, 78]. To circumvent the issue of excessive formation of the passivation layer, a common way is to treat the surface by coating with precious metal (e.g. Pt) as a protective layer through magnetron sputtering or alloying [79–82], but this method increases the overall cost of the electrode. To this end, Bystron *et al* proposed an alternative method of reducing the extent of passivation based on the chemical etching of Ti in the HCl aid and investigated the influence of appropriate treatment of Ti surface on the surface contact resistance and the cell performance [77]. The surface of Ti was modified by HCl etching to form a Ti hydride underlayer to grant the metal surface improved resistance to excessive passivation. More importantly, the surface contact resistance was reduced after the treatment, with its tendency to increase suppressed even during water electrolysis for more than 100 h at 1 A cm^{-2}. Besides, the passivation can also be suppressed by depositing a suitable catalyst that also improves the electrochemical performance. For instance, Doan *et al* applied spray coating and thermal treatment, and a thin layer of IrO_2/TiO_2 catalyst was formed on the surface of Ti PTL to prevent surface passivation [76]. Simultaneously, the performance of PEMWE was enhanced as the cell ohmic resistance was reduced due to the prevention of TiO_2 formation.

3.2. Membrane modification

The well-established perfluorosulfonated acid (PFSA) membranes represented by the Nafion membranes are characterized by high proton conductivity, excellent mechanical strength, and good chemical stability [83]. However, there are efficiency and safety issues (especially with hydrogen flammability limit of 4% H_2 concentration in O_2 at ambient conditions) since the PEM allows significant permeation of gaseous products, especially when the thickness of the membrane is decreased to reduce cell resistance [84, 85]. Moreover, degradation of the membrane will largely deteriorate the cell performance and durability because the membrane is prone to chemical attack by trace radical species such as hydroxyl radicals in the presence of H_2, O_2, and Pt [86]. The degradation of membranes can then cause kinetic deactivation and irreversible resistive losses that are one order of magnitude higher compared to the kinetic losses [87]. Hence, developing modification strategies of enhancing the lifetime and mitigating the gas crossover issue is instructive to further promote the performance of PEMWE.

In addition to PFSAs, hydrocarbon membranes are promising candidates since they are fluorine-free and have less gas crossover and lower production costs [88, 89]. Nevertheless, they are less stable because the carbon-hydrogen bonds are weaker than the carbon-fluorine bonds of PFSA [90]. Klose *et al* prepared a fully hydrocarbon-based MEA with sulfonated poly (phenylene sulfone) (sPPS) acting as both membrane material and ionomer binder in the electrode for water electrolysis, where sPPS had an equivalent weight of 360 g eq^{-1} and ion exchange capacity of 2.78 meq g^{-1} [91]. The sPPS-MEA reached a higher current density of 3.48 $\pm$ 0.03 A cm^{-2} at 1.8 V (figure 6(a)), outperforming the MEA using Nafion 115 with the same catalyst loading (1.5 A cm^{-2} at 1.8 V), which is the result of the 60% lower high-frequency resistance (HFR) (161 $\pm$ 7 mΩ cm^2) for sPPS. With hydrogen crossover current density below 0.3 mA cm^{-2}, pure sPPS-membranes exhibited only a third of hydrogen crossover current density of Nafion 115 membranes in a fully humidified surrogate test, enabling safe operation at lower current densities and resulting in a larger predicted operational current density range of sPPS-MEA (figure 6(b)). However, the durability of sPPS-MEA hindered its commercial adoptability due to membrane softening caused by high water content and degradation caused by increased crossover. Likewise, Park *et al* developed a hydrocarbon-based

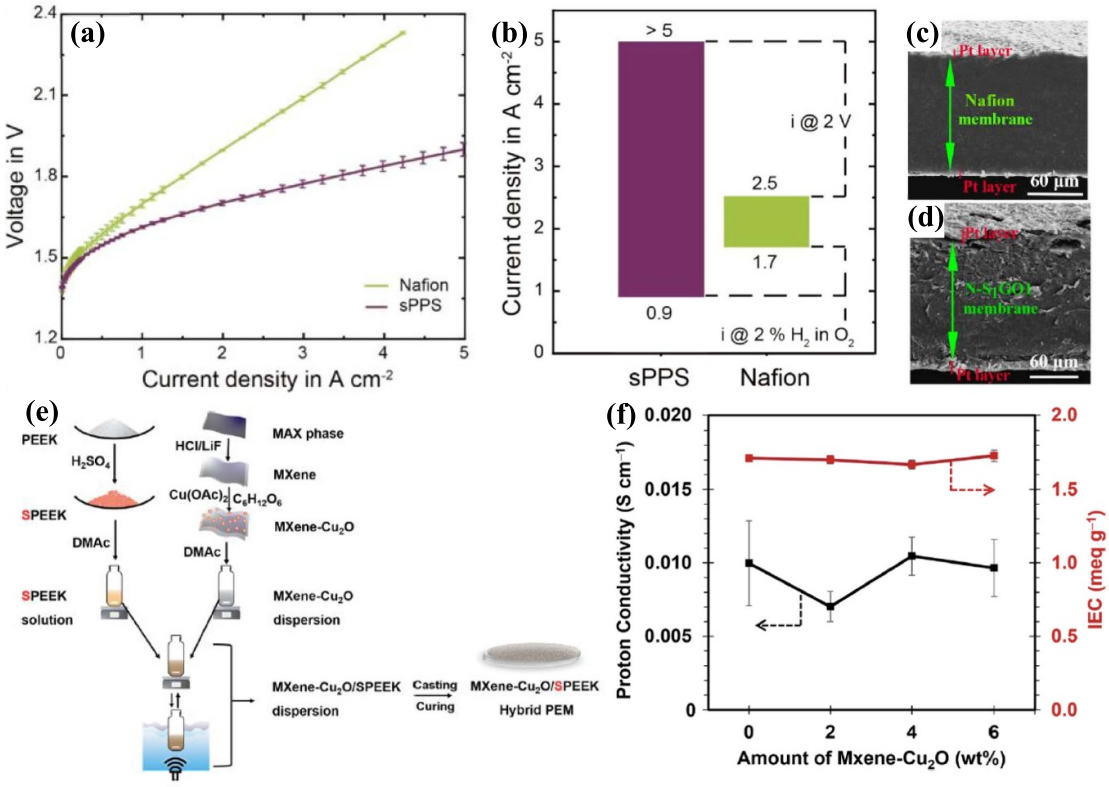

Figure 6. (a) The cell polarization of Nafion-MEAs and sPPS-MEAs, and (b) the estimated operational current density range of a theoretical sPPS-based electrolyzer and an Nafion 115-based electrolyzer. Reproduced from [91]. CC BY 4.0. © 2020 The Authors. Published by WILEY-VCH Verlag GmbH & Co. KGaA, Weinheim. The cross-sectional field emission scanning electron microscopy (FESEM) images of (c) N.$Pt_{5.2}$ and (d) N.SGO_1.$Pt_{5.2}$. Reprinted from [98], Copyright (2021), with permission from Elsevier. (e) Schematic illustration of synthesizing MXene Cu_2O/SPEEK membrane and (f) comparison of ion exchange capacity (IEC) and proton conductivity between SPEEK and composite membranes with different weight percentages of MXene-Cu_2O. Reprinted from [99], Copyright (2022), with permission from Elsevier.

membrane and ionomer for PEMWE, using sulfonated poly (arylene ether sulfone) with a degree of sulfonation of 50 mol.% (SPAES50) synthesized via condensation polymerization [92]. They evaluated the influence of different membrane thicknesses (20, 30, and 40 μm) and ionomer contents (5, 10, 20, 30 wt%). The 5 wt% and 10 wt% ionomer contents in the anode and the cathode, respectively, gave the best PEMWE performance owing to the optimal charge transfer resistance since the cell performance was largely influenced by the blockage of the active sites by the excessive ionomer content. Moreover, the hydrogen crossover issue was resolved in a SPAES50 membrane with a thickness of 20 μm as smaller channel size reduced hydrogen permeation, indicating its potential in replacing the thicker Nafion 115 with a similar hydrogen crossover. By optimizing the membrane properties, the current density reached 1069 mA cm^{-2} at 1.6 V, exceeding those of Nafion-based PEM with thicknesses of 25 μm and 125 μm.

Moreover, there are more novel membrane materials emerging in recent years, such as adding an appropriate amount of nanofillers into the initial polymer material to make composite membranes to enhance the production performance [93–96]. For example, graphene-based nanofiller is very versatile, being a popular reinforcing agent in enhancing mechanical properties, thermal stability, electrical conductivity, and gas barrier property of polymer matrices in a wide range of applications [97]. Mahdi *et al* prepared a Nafion/sulfonated graphene oxide (SGO) nanocomposite membrane for deposition of the catalyst with low loading [98]. The nanocomposite membrane was synthesized by solution casting, followed by coating Pt nanoparticles on the surface (N.SGO.Pt) through the electroless deposition method by varying the mass ratio of sulfanilic acid/GO and Pt salt solution concentration. The cross-sectional image (figures 6(c) and (d)) suggested the successful deposition of Pt catalyst on pure Nafion membrane and optimal N.SGO_1.$Pt_{5.2}$ nanocomposite membrane with slightly higher Pt layer thickness. This is because the high level of ion exchange site, $-SO_3H$ groups, introduced by SGO, provided more nucleation sites for Pt^{2+} ions to adsorb and grow into Pt nanoparticles, thereby leading to higher penetration of Pt nanoparticles into the membrane and better distribution on the membrane surface.

In addition, the use of MXene in PEMWE is noteworthy since MXene as a rising star of 2D material featured for its excellent conductivity, high strength, and hydrophilic nature [99, 100]. Considering p-type

semiconductor Cu_2O is a potential filler with superhydrophilic nature to enhance the ionic conductivity, MXene coupled with Cu_2O was prepared by Waribam *et al* to serve as filler in the sulfonated polyether ether ketone (SPEEK), a hydrocarbon-based polymer, to make a novel PEM for water electrolysis [99]. This hybrid MXene-Cu_2O/SPEEK membrane was fabricated by a simple solution casting method to disperse the MXene-Cu_2O composites into the SPEEK matrix (figure 6(e)). In detail, MXene was synthesized by HF-etching the Ti_3AlC_2 MAX, followed by adding copper precursors to obtain MXene-Cu_2O composites. Through constructing a hybrid membrane, the proton conductivity of the membrane was enhanced compared to the pristine PEEK membrane, with the highest value of 0.0105 S cm^{-1} achieved in 4%MXene-Cu_2O/SPEE (figure 6(f)), which was due to the uniform distribution of composite for the formation of hydrogen bonds, bringing about higher H_2 evolution volumetric flow rate. The formation of hydrogen bonding between the SPEEK polymer and MXene-Cu_2O composite was also the key to reducing the swelling area in the membrane.

Besides material selection of the membrane, the selection of membrane fabrication method, which relies on the polymer chosen and the desired structure [101], is also critical in improving PEMWE efficiency by reducing interfacial resistance, degradation and cost. For instance, Siracusano *et al* compared the Aquivion membranes with an equivalent weight of 980 g eq^{-1} and a thickness of 90 μm manufactured using extrusion and casting methods [102]. While both had low gas permeability at current density of 1–4 A cm^{-2} and a differential pressure of 20 bar and their respective MEAs exhibited a voltage efficiency of over 80% (versus thermoneutral potential) at high current densities (3–4 A cm^{-2}) and high temperatures (80 °C–90 °C), the recast membrane showed smaller surface roughness, increasing the contact area between the ionic cluster of the membrane and CLs. Hence, in the activation region of the polarization curves, the recast membrane slightly outperformed the extrusion membrane. However, the recast membrane had higher polarization resistance but lower series resistance at 1.8 V and in low-temperature operating conditions.

Generally, attempts have been made to optimize the physicochemical and mechanical properties of both PEM and the electrodes through various modification strategies and tuning of the operating conditions. While novel membranes are introduced to replace the conventional PEM, modifications of the electrode discussed here are mostly focused on enhancing the interaction between PTL and CL and tuning of the properties of PTLs or GDLs. In particular, regulating the porosity, durability, and conductivity of PTLs is overriding since it is the primary location for mass and electron transport.

4. Catalysts for PEM water electrolysis

Currently, the cost of catalysts in the PEMWE system is relatively small, accounting for around 5% [11, 103, 104]. Nonetheless, as the system scales up to the MW or GW-based stack power, the contribution of the catalyst in the production cost becomes more significant while the contribution of balance-of-plant cost is expected to be minor [103]. As such, the transition from the gold-standard platinum group metal (PGM) catalysts to PGM-free or PGM with noticeably reduced loading is pressing. The industrial benchmark loadings of Pt/C catalyst for HER and IrO_2 for OER are 0.5–1.0 mg_{Pt} cm^{-2} and 2 mg_{Ir} cm^{-2}, respectively [105]. The amount of platinum loading can be feasibly reduced (by an order of magnitude) without significantly reducing the performance due to the high kinetics of HER on the cathode side in the acidic environment, but it is difficult to reduce the loading of iridium catalyst without significantly reduce the efficiency at the same current density since the anode is usually the kinetic bottleneck [106, 107]. Numerous efforts have been devoted to reducing the catalyst loading as well as employing catalyst other than PGMs in the MEA system to obtain a feasible result under practical device conditions, which will be discussed in this section.

4.1. Catalysts for HER

Improving HER catalysis is typically achieved through either reduction in PGM loading or replacement of PGMs with either transition metal-based catalysts or molecular catalysts. Reduction in PGM loading can be achieved by optimizing CL thickness and employing suitable support material, whereas transition metal-based catalysts are improved by morphological control, employing porous shell structures, sulfidation, modification and electrodeposition.

4.1.1. Optimizing PGM content

Many synthesis strategies have been deployed to minimize Pt catalyst loading, such as atomic layer deposition, electrodeposition method, sputter deposition method, modified thin-film methods, wet chemistry method, and annealing [108–110]. For example, Wang *et al* successfully reduced Pt catalyst loading to only 0.003 79 mg cm^{-2} by using direct electron beam (e-beam) evaporation deposition on Nafion membrane, forming a highly uniform Pt thin film with low surface roughness and an optimal thickness of

6 nm that was evenly distributed on the membrane [111]. Its current density reached 500 mA cm^{-2} at 1.64 V under 80 °C, which was competitive with Pt/C-based MEA. Its low thickness was sufficient to lower the mass transport loss, thus reaching a balance between maximizing the amount of active sites and preventing blockage of proton diffusion channels in the membrane by the deposited thin film. When the temperature was increased from 20 °C to 80 °C, the catalytic activation barrier could be further reduced while increasing proton transportation rate, dramatically increasing the current density from 483 to 855 mA cm^{-2} at 1.75 V.

HER on PGM catalysts can also be improved by improving the carbon support, particularly through doping. Kumar and Himabindu reported a MEA containing boron-doped carbon nanoparticles supported 30 wt% Pd as the cathode catalyst synthesized by chemical vapor deposition method, which exhibited a high stability of up to 500 h at 1 A cm^{-2} under a temperature of 80 °C [112]. B doping improved the conductivity of the carbon support by increasing the density of charge carriers. The cell voltage of the fabricated MEA decreased while the cell efficiency increased (up to 72%) at higher temperatures up to 80 °C owing to the promoted HER kinetics at a higher temperature, thus delivering similar performance to 30 wt% Pt supported on carbon black and having higher cost efficiency than Pt.

4.1.2. Transition metal-based catalysts

One way to replace PGM is by using corrosion-resistant noble metals such as Ag. A robust catalyst that exhibits insignificant degradation under high operational cell voltage can be produced by controlling the morphology and subsequently, the exposed facets of the catalyst, proton availability and H atom coverage can be tuned to significantly improve HER efficiency. Mo *et al* prepared a series of silver catalysts with different morphologies, namely nanocubes, nanowires, and nanospheres [113]. While the Ag catalyst was inferior to the Pt/C catalyst over a potential range of −1.0 to −2.0 V in the electrolyzer, the Ag nanocubes delivered the highest current density (3.5 A cm^{-2}) when a more negative potential of −2.5 V was applied, exhibiting a potential for upscaling. More H atoms were readily absorbed on the metal surface at a more negative applied potential, causing a change in the rate-determining step (RDS) from the Volmer step to the Tafel step. The Ag–H bonds at the Ag nanocube surface were weaker than Pt–H bonds, favoring H migration and the H_2 formation, thereby increasing the H_2 productivity.

Transition metal-based catalysts, including transition metal chalcogenides, phosphides, nitrides, and alloys, are also promising candidates for HER catalysis, having demonstrated decent HER activity in the acidic environment [114]. Besides, early transition metals are more abundant (with around 2–3 orders of magnitude higher estimated concentration in Earth's crust) and cheaper than PGMs [106, 115]. On account of unfilled d orbitals in transition metals, their properties are prodigiously different from other metals [116]. Feng *et al* prepared ultrafine tungsten carbide (WC) nanocrystals encapsulated in porous N-doped carbon nanosphere (NC) through a facile and scalable one-step pyrolysis method to obtain WC@NC [117]. As demonstrated in SEM images (figures 7(a) and (b)), WC@NC had a uniform, grape-like, monodisperse nanosphere morphology. Besides, the WC nanoparticles were wrapped in N-doped carbon shells which was critical in confining the WC nanoparticles, thus preventing active ingredients from leaching in the harsh operating environment while improving electrical conductivity. This structure was favorable in optimizing the H-binding energy, thus boosting its HER activity and stability in both acid and alkaline environments when tested in the half-cell system. In the single-cell test for performance evaluation, a CCM was prepared for MEA with WC@NC and IrO_2 acting as the cathode and anode, respectively. The best performance was achieved at 80 °C, with a voltage of 2 V delivering a current density of 0.78 A cm^{-2} (figure 7(c)). However, low durability was observed at over 12.5 h in this MEA system, which might be due to metallic cation poisoning, CL detachment, and catalyst dissolution. Similarly, the significance of incorporating carbon materials in transition metal-based HER electrocatalysts was also demonstrated by Morozan *et al*, where combining FeMoS with carbon nanotubes resulted in higher HER activity, exhibiting its suitability as a cathode catalyst in MEA for PEM electrolyzer single cell operation [118].

Additionally, Kim *et al* have prepared a transition metal oxysulfide ($Ni_yCo_{1-y}O_xS_z$) cathode, which was directly grown on the carbon paper (CP) [37]. A two-step electrodeposition coupled with anion exchange methods was applied to control the morphology and composition of the catalyst, where the $Ni_yCo_{1-y}O_x$/CP was first synthesized with shapes varying from sphere to fern-like shape, followed by a sulfidation process to partially replace the O atoms with S to obtain $Ni_yCo_{1-y}O_xS_z$/CP catalyst. Both the plots of intrinsic activity normalized by ECSA as functions of S surface composition and proportion of S atoms having higher binding energies displayed 'volcano plot' behaviors (figures 7(e) and (f)), in which $Ni_{0.78}Co_{0.22}O_xS_{0.25}$/CP outperformed other catalysts in terms of intrinsic activity, emphasizing the critical role of S composition in influencing its intrinsic HER activity. In PEMWE, $Ni_{0.64}Co_{0.36}O_xS_{0.28}$/CP was determined to be a suitable cathode catalyst in MEA for practical operation owing to the lowest overpotential obtained from the preceding three-electrode cell system, with IrO_2/CP as the anode. At the cell voltage of 2.0 V, the PEMWE

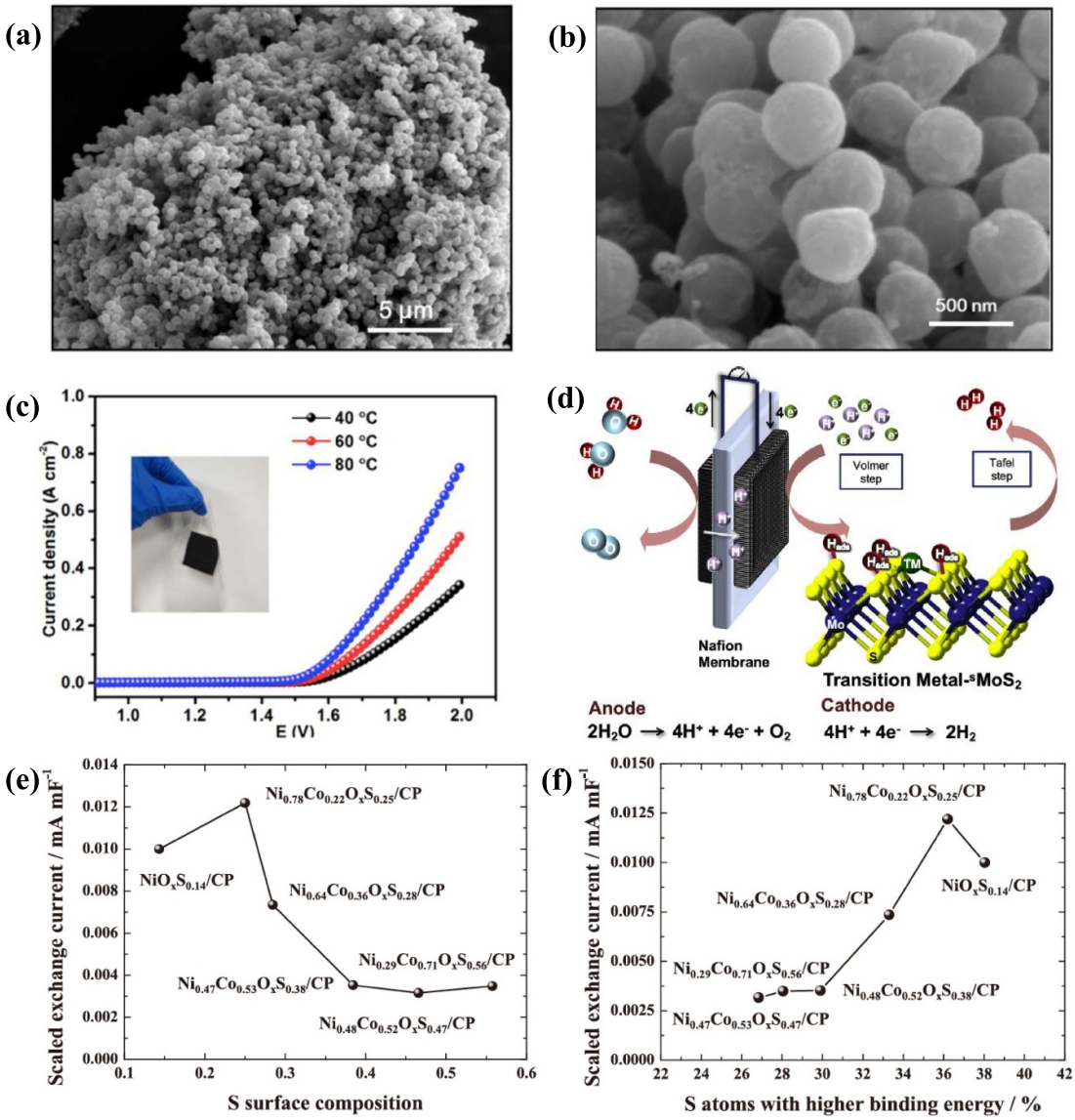

Figure 7. SEM images of WC@NC at (a) low and (b) high magnifications, and (c) polarization curves of the single cell using WC@NC as the cathode tested at different temperatures (inset: prepared CCM). Reprinted with permission from [117]. Copyright (2019) American Chemical Society. (d) Schematic illustration of a PEM electrolyzer using TM-$^{S}MoS_{22}$ as cathode catalyst and IrO_2 as anode catalyst. Reproduced with permission from [119]. © 2019 Published by Elsevier Ltd. Plots of scaled exchange current as functions of (e) S surface composition and (f) fraction of S atoms with higher binding energy. Reprinted from [37], Copyright (2018), with permission from Elsevier.

reached a current density of 0.72 A cm^{-2}. The relationship between S atoms with higher binding energy and the HER intrinsic activity is in agreement with another study, in which an amorphous MoS_x catalyst was electrodeposited on the CP as a cathode in the electrolyzer [120]. In this system, the impacts of deposition potential and deposition times were also uncovered, wherein the deposition time showed more significant influence, especially in the crack and crevice formation at highly negative deposition potential in excessive deposition durations, causing undesired aggregation of catalyst on the surface.

Furthermore, appropriate modification strategies can be applied to TM-based catalysts to further optimize the catalytic activity and rectify their existing shortcomings such as unsatisfactory conductivity and unregulated electronic structure [116]. For example, though MoS_2 has a free energy of hydrogen adsorption (ΔG_H) similar to that of Pt due to the active edge sites for HER, the basal planes of MoS_2 are EC inactive [121, 122]. Mo *et al* decorated single transition metal atoms (TM = Fe, Co, Ni, Cu) on the basal planes of single-layer MoS_2, thus creating more active sites by activating the inert basal plane [119]. The single TM atoms were doped in the position of Mo atop sites. Among all the TM-modified systems, the tetrahedral anchored Co in the absence of the Co–Mo bond induced a proper downshift of the conduction band so as to endow the S sites the with highest HER activity. As a result, the Co-$^{S}MoS_2$ exhibited the best catalytic performance among other studied transition metal doped systems when tested in a PEMWE with Nafion 115

membrane as the PEM and IrO_2 as the anode catalyst (figure 7(d)) at an applied cell potential of −1.0 V to −2.4 V. An even higher performance of molybdenum sulfide-based HER catalyst was achieved by Holzapfel *et al*, where $[Mo_3S_{13}]^{2-}$ nanoclusters were supported on nitrogen-doped carbon nanotubes (Mo_3S_{13}-NCNT) through a self-assembly process attributed to the high affinity of Mo atoms to N atoms with higher electronegativity in CNTs [123]. This catalyst delivered a superior current density of 4 A cm^{-2} at a cell voltage of 2.36 V (figure 8(a)) due to the EC induced activation process of the catalyst at high current density. The electrochemical performance in MEA enhanced dramatically during the cell activation process (figure 8(b)), particularly when applying Nafion 212 membrane with a smaller thickness that was able to lower ohmic resistance, resulting in a significant increase in the current density by 908 mA cm^{-2} at 2.2 V. Moreover, there was only a small degradation rate of 83 μV h^{-1} ascribed to the increased HFR-free cell voltage during a stability test of 100 h at 1 A cm^{-2}, exhibiting a stable polarization behavior.

It is noteworthy that the electrodeposition method is broadly used in fabricating the catalyst for use in the electrode because of its inherent benefit of achieving high catalyst utilization [109, 125]. For example, Choi *et al* prepared a CuNiMo ternary alloy by rapid electrodeposition, which allowed the direct and simple fabrication of a catalyst on CP for use as a PTL in PEMWE [126]. $Cu_{44.4}Ni_{46}Mo_{9.6}$ was the optimal ternary alloy with increased surface area, in particular, showing a double layer capacitance of 125 mF cm^{-2}, much higher than that of the single metal and binary alloy catalysts studied. The PEMWE single cell system using $Cu_{44.4}Ni_{46}Mo_{9.6}$ exhibited no degradation after operation for 48 h. In terms of the cost, the cost efficiency of the MEA using $Cu_{44.4}Ni_{46}Mo_{9.6}$ was at least 190% higher than those of previously reported MEA using PGM catalysts. In this system, the synergy between the components in $Cu_{44.4}Ni_{46}Mo_{9.6}$ made a significant change in the active surface area, intrinsic activity, and durability, rendering it a cost-effective ternary catalyst for future commercial application. Similarly, the synergic effect among metals in the alloy and even with the metallic support has also been discovered by Kim *et al*, who synthesized a transition metal alloy NiMo catalyst supported by Cu foam deposited on CP (NiMo/CF/CP) through electrodeposition [127]. The CF with a highly roughened surface served as a support for NiMo electrocatalysts in order to obtain a large electrochemical surface area and enhanced the mass transfer. With CF as support, the overpotential was reduced from 297.9 mV to 68.7 mV at −10 mA cm^{-2}, signifying the importance of metallic support in this study. The PEMWE using NiMo/CF/CP as the cathode achieved a remarkable current density of ∼2.0 A cm^{-3} at 2.0 V, but it was lower than that using the Pt/C as the cathode catalyst. On top of that, electrodeposition is also capable to control the size and distribution of the catalyst on the conductive support by adjusting the operating parameters. Yoon *et al* reported an acid-durable cobalt phosphide (Co–P) catalyst synthesized via pulse electrodeposition on CP, where the P content was controlled by adjusting the applied dissolution potential [128]. The acid durability of the best-performing Co–P catalyst (Co–P-0.3, synthesized using dissolution potential of −0.3 V_{SCE}) was evaluated in 0.5 M H_2SO_4 through an accelerated degradation test (ADT) comprising 500 cyclic voltammetry (CV) cycles. The recorded linear sweep voltammetry (LSV) curves for 500 ADT cycles suggested that the performance of the Co–P-0.3 catalyst remained relatively stable with a non-negligible deviation found after 500 CV cycles marked by an increase in overpotential of only 43.73 mV and the lack of change in the surface morphology.

Although electrodeposition is widely applied, limitations such as aggregation issues and susceptibility of the formed porous structure to degradation under cell operation conditions still exist [125], discouraging the industrial adaptation of this approach. Therefore, exploring the scalability of this method would be profound, and fortunately, works have been done in this aspect. For instance, Wei *et al* proposed a scalable and facile electrodeposition method in ethaline-based deep eutectic solvent employing a sacrificial anode set-up to synthesize NiFe-based electrocatalysts for the investigation of industrial water electrolysis [129]. In this method, different catalytic electrodes were prepared by simply adjusting the composition of the electrolyte, and simultaneously, the energy consumption, the potential system decomposition, and the contamination of the anode could be reduced by introducing Fe anodes as Fe sources.

4.1.3. Molecular catalysts

In addition to heterogeneous catalysts, the potential of molecular catalysts is also tapped because of the tunability of their catalytic activity and selectivity through modifying geometry of their ligand structure [130], contributing to realizing an applicable MEA under practical conditions. For instance, the remarkable stability of a HER catalyst in a PEM water electrolyzer was realized by Bellini *et al*, in which a dinuclear Ru diazadiene olefin complex, $[Ru_2(OTf)(\mu\text{-H})(Me_2dad)(dbcot)_2]$, supported on carbon black was employed as the cathode to produce hydrogen (28 L_{H2} min^{-1} g_{Ru-1}) with a current density of 400 mA cm^{-2} at 1.9 V and 80 °C [131]. An excellent turnover frequency of 7800 mol_{H2} $mol_{catalyst}{}^{-1}$ h^{-1} was maintained over a week of operation at 0.2 A cm^{-2} and a temperature of 80 °C, showing the predominant stability of this device. This could be traced back to the inherent ligand framework comprising exclusively stable C–C, C–N, and C–H bonds without any sensitive components that caused catalyst deactivation.

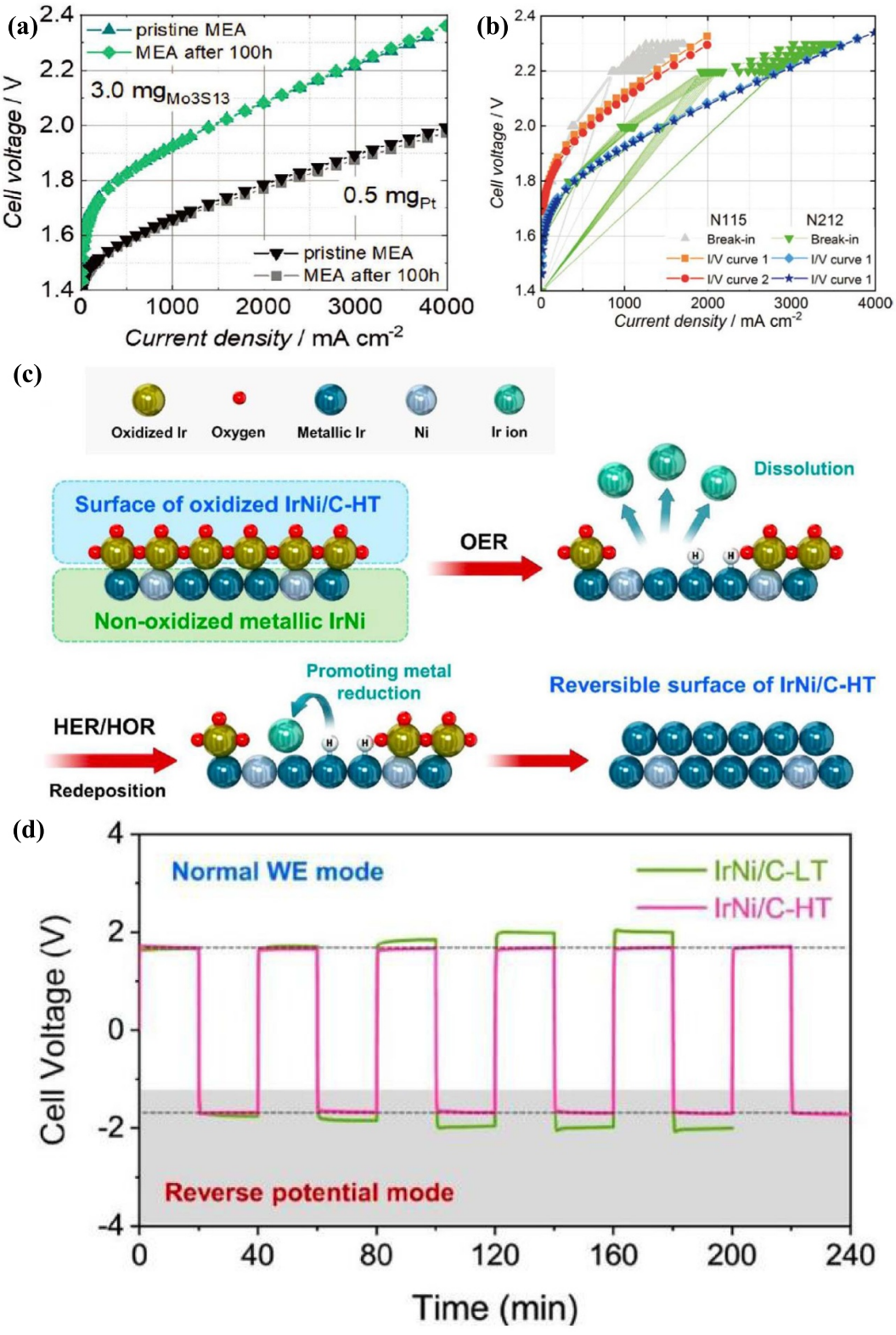

Figure 8. (a) Polarization curves of the pristine MEAs and MEA after the 100 h durability test, comparing Mo_3S_{13}-NCNT cathode with Pt/C reference, and (b) full cell activation procedure and polarization curves using Mo_3S_{13}-NCNT based cathodes with catalyst loading of 3 mg $[Mo_3S_{13}]^{2-}$ cm^{-2} in MEAs using Nafion 115 or Nafion 212 membrane. [123] John Wiley & Sons. © 2020 The Authors. Published by Wiley-VCH GmbH. (c) The dissolution and re-deposition mechanism of IrNi/C-HT under OER-HER conditions, and (d) comparison between IrNi/C-LT and IrNi/C-HT in a reverse voltage experiment in a single water electrolyzer with 10 cm^2 geometric area at a current density of 40 mA cm^{-2}, operating under intermittent switching between cathodic and anodic processes. Reproduced from [124], with permission from Springer Nature.

4.1.4. Hydrogen evolution-oxidation bifunctionality

The advanced design of MEA can be aimed at integrating fuel cell and electrolyzer into a single cell, for which the voltage reversibility of the integrated cell has to be improved to prevent induction of a large positive

potential on the hydrogen electrode and severe system degradation [132–134]. This design is particularly useful in practical operations when there is a sudden power outage during water electrolysis or fuel starvation in the fuel cell. Lee *et al* designed a highly crystalline Ir-based alloy electrocatalyst to improve the kinetics of OER, HER, and hydrogen oxidation reactions (HORs) simultaneously, in which the carbon-supported IrNi alloy nanoparticles with high crystallinity (IrNi/C-HT) were synthesized [124]. Under OER operation, the crystalline nanoparticles generated an atomically thin $IrNiO_x$ layer on IrNi/C-HT, the number of d-band holes of which experienced a significant increase during OER, resulting in excellent OER catalytic activity. Under HER/HOR operation, this thin IrO_x layer was reversibly transformed into a metallic surface, exhibiting high catalytic activity for HER/HOR. Therefore, the key to the reversibility is the thin $IrNiO_x$ layer, which was generated via dissolution and re-deposition mechanism (figure 8(c)), where the metallic surface was formed after $IrNiO_x$ dissolution under HER condition and re-deposition of the dissolved Ir ions occurred when metallic surface served as a substrate to accelerate the reduction of Ir ions to metal under HER/HOR condition, promoted by the adsorbed hydrogen. In the MEA system, the IrNi/C-HT catalyst exhibited high reversibility and maintained its bifunctional catalytic activity for HER/OER and HOR/OER even after 10 polarity conversions (up to 240 min) (figure 8(d)).

Summarily, the search for alternative HER catalysts is on the spotlight in recent years (table 1), especially through developing transition metal-based electrocatalysts, which is more appealing than manipulating the content of Pt by adding support and applying well designed synthesis methods. However, most of the transition metal-based catalysts investigated in MEA are still inferior to the benchmark noble-metal catalyst, implying that the recent novel catalyst is yet to be capable of realizing industrial standard water electrolysis. The benchmark Pt/C performance is more frequently exceeded by other PGMs, and hence, the reliance of the technology on PGMs is not expected to be eliminated in near future.

4.2. Catalysts for OER

Minke *et al* have demonstrated that the scarcity of iridium element makes its current demand unsustainable for a commercial PEMWE market with a production rate of about 7 t a^{-1} [107]. It is suggested that the loading of iridium catalyst in PEMWE cells needs to be dramatically reduced to a target loading of 0.05 g kW^{-1} by 2035. Enhancing OER catalysis can be done by incorporating suitable support material and employing better catalysts.

4.2.1. Support materials

In reducing Ir loading, employing suitable support is the most used strategy that enhances the coordination between catalyst and support as well as electrical conductivity by utilizing conductive materials as the substrate. Carbon-based materials are commonly used as support due to their large surface area, good electric conductivity, and porous structure [137, 138]. However, the materials used at the anode of PEMWE must withstand an acidic ($0 < pH < 1$) and oxidizing environment (with anodic potential above 1.5 V versus reversible hydrogen electrode, RHE) [139]. As carbon-based materials are prone to carbon corrosion and performance deterioration in OER, developing alternative support materials is necessary.

Corrosion-resistant TiO_2 support can effectively lower the loading of precious metal catalysts while endowing the system with stable catalytic activity during PEMWE operation due to its surface that is favorable for catalyst dispersion, requiring only minimum amount of IrO_2 nanoparticles to form a conductive network [140, 141]. Regmi *et al* reported a core–shell design by depositing a conformal layer of Pt nanoparticles on the TiO_2 core by photoreduction to prepare conductive layer-coated supports (CCSs), followed by dispersing Ir catalyst on the CCSs using wet impregnation method [142]. This semiconductor-assisted photon-driven reduction facilitated the formation of evenly distributed Pt nanoparticles on the TiO_2 surface with strong inter-particle interaction to prevent the aggregation of nanoparticles when coated with the Ir catalyst in the subsequent process. By inserting the Pt interlayer, the direct interaction between Ir and Ti was avoided, resulting in high stability of the Ir surface. Even after annealing, Ir still retained its metallic character due to efficient charge transfer from Ir to Pt. As a result, the conductivity of the catalyst with significantly decreased Ir loading (39 wt%) was higher than that of commercial IrO_2–TiO_2 catalyst with 75% loading, further contributing to superior performance in the MEA (1.87 V at 1 A cm^{-2}) despite being inferior to the unsupported IrO_x catalyst. Moreover, the performance can be improved by direct modification of TiO_2. For example, Min *et al* developed the homogeneously depressed IrO_x catalyst through surface modification and Ir-controlled hydrolysis on W-doped TiO_2 support [143]. The resultant MEA reached a low cell voltage of 1.602 V at 1 A cm^{-2} with a low Ir loading (IrO_x: 0.116 mg cm^{-2}), which was superior to the performance of benchmark IrO_2 and 20% IrO_x/TiO_2 (IrO_x: 0.82 mg cm^{-2}), demonstrating performance enhancement through W doping. In a more complex engineering strategy, Lv *et al* engineered the TiO_2 support by doping Nb ions and creating O vacancies ($Ti_{0.9}Nb_{0.1}O_{2-x}$, TNO) via a modified evaporation-induced self-assembly method and a subsequent hydrogenation process [144]. This

Table 1. Representative summary of HER cathode catalyst in MEA.

Cathode catalyst	Fabrication method	GDL/PTL	Membrane	Electrochemical performance	Catalyst/noble metal loading	Stability	References
30 wt% Pd/B-CNPs	CCM	N/A	Nafion 115	2.04 V@1 A cm^{-2} 2.32 V@2 A cm^{-2}	3 mg cm^{-2} (30 Pd wt%)	>500 h@1 A cm^{-2}	[112]
WC@NC	CCM	N/A	Nafion 212	0.78 A cm^{-2}@2 V	4.2 mg cm^{-2}	>20 h@0.2 A cm^{-2}	[117]
FeMoS (mw)	CCM	Carbon-based GDL	Nafion 212	1.85 V@1 A cm^{-2}	0.24 mg cm^{-2}	AST for 24 h, cycled between 0.05 A cm^{-1} and 0.5 A cm^{-1} and held at each intensity for 15 min.	[118]
20 wt% Ag cubes/C	CCM	CP	Nafion 211	3.439 A cm^{-2}@2.5 V	0.4 ± 0.05 mg cm^{-2} Ag	>500 h@-2.5 V	[113]
Pt	CCM	CP	Nafion 117	0.5 A cm^{-2}@1.64 V	0.003 79 mg cm^{-2} Pt	N/A	[111]
$Ni_{0.64}Co_{0.36}O_xS_{0.14}$	GDE	CP	Nafion 212	0.72 A cm^{-2}@2.0 V	N/A	N/A	[37]
Mo_3S_{13}-NCNT	GDE	Carbon cloth PTL	Nafion 212	2.36 V@4 A cm^{-2}	1.5 mg cm^{-2} $[Mo_3S_{13}]^{2-}$	>100 h@1 A cm^{-2}	[123]
NiMo/CF	GDE	CP	Nafion 212	2.0 A cm^{-2}@2.0 V	N/A	>36 h@2.0 V	[127]
L-$Ni_{0.4}6P_{0.54}$	GDE	CP	Nafion 212	1.47 A cm^{-2}@2.0 V	N/A	>16 h@1.0 A cm^{-2}	[135]
Single TM atom (Fe, Ni, Co, Cu)-doped sMoS_2	CCM	CP	Nafion 115	2.1 V@1 A cm^{-2} for Co-sMoS_2	4.5 ± 0.25 mg cm^{-2}	N/A	[119]
$[Ru_2(OTf)(\mu\text{-H})(Me_2dad)(dbcot)_2]$@C	GDE	CC	Nafion 117	345.5 mA cm^{-2} @ 2.2 V	0.043 mg cm^{-2} Ru	>168 h@200 mA cm^{-2}	[131]
Co–P-0.3	GDE	CP	Nafion 212	1.89 A cm^{-2}@2.0 V	6.12–6.19 mg cm^{-2}	N/A	[128]
Au/C	CCM	Platinized titanium fiber felt	Nafion 117	2.32 V@1 A cm^{-2}	0.5 mg cm^{-2}	N/A	[136]
$Cu_{44.4}Ni_{46}Mo_{9.6}$	GDE	CP	Nafion 212	1.62 A cm^{-2}@1.9 V	1.33 mg cm^{-2}	>48 h@1.9 V	[126]
MoS_x	GDE	CP	Nafion 212	0.37 A cm^{-2}@1.9 V	0.13 mg cm^{-2}	>4 h@1.9 V	[120]
PtNW	GDE	Ti LGDLs	Nafion 115	1.643 V@1 A cm^{-2}	0.2 mg cm^{-2}	N/A	[64]

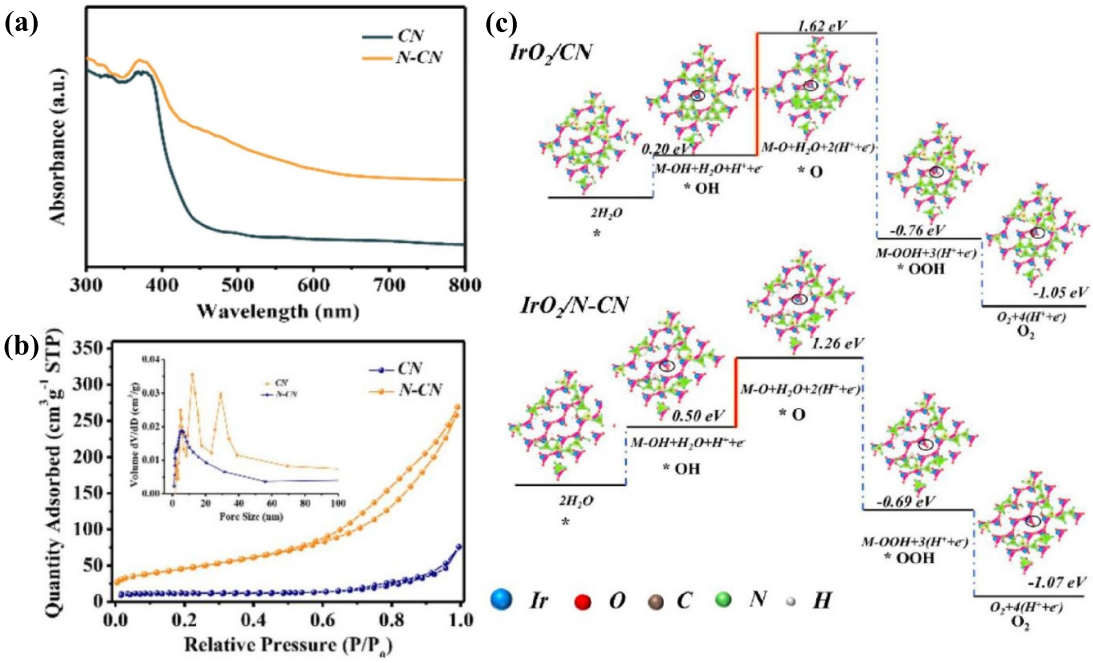

Figure 9. (a) UV–Vis diffuse reflection spectra of IrO_2/CN and IrO_2/N–CN, (b) N_2 adsorption-desorption isotherms of IrO_2/CN and IrO_2/N–CN (inset: pore-size distribution curves), and (c) the free energy diagrams of the OER process on IrO_2/CN and IrO_2/N–CN. Reprinted with permission from [149]. Copyright 2021, Elsevier.

two-pronged approach increased the electrical conductivity and the amount of surface active sites to promote OER kinetics. The oxygen vacancies behaved as charged species and facilitated the charge transfer process. With a low Ir mass loading, MEA single cell integrated with the optimal IrO_2/TNO anode presented a voltage of 1.832 V at 1 A cm^{-2}, which is lower than that with unsupported IrO_2 (1.858 V at 1 A cm^{-2}) and exhibited good stability during the 100 h operation at 1 A cm^{-2} in a single cell.

Another group of suitable support materials comprise of two-dimensional (2D) nanomaterials possessing unique geometric and electronic properties owing to their large surface area with abundant active sites, atomic-scale thickness, excellent mechanical properties, and tunable surface chemistry, thus having the promise of serving as excellent substrates to stabilize catalysts [145, 146]. For example, graphitic carbon nitride has a 2D graphite-like structure with the tri-s-triazine unit as the building block. It is a metal-free and cost-effective substrate for OER catalysts to confine the catalyst through strong electronic interaction induced by C or N atoms, simultaneously decreasing the catalyst loading and maximizing the exposure of active sites [147, 148]. Wang *et al* introduced N defect into the g-C_3N_4 (N–CN) that acted as a catalyst substrate for IrO_2 nanoparticles [149]. N defects in CN regulated the extra electrons to the closest C atoms along with increased π-electron delocalization in a conjugated network of CN, thereby supplying more electrons to IrO_2. The change in the electronic structure of CN was verified by the UV–Vis diffuse reflection spectra, where the light absorption was enhanced for N–CN relative to CN (figure 9(a)) stemming from the boosted π-electron delocalization in N–CN. Besides, the porous structure with larger pore size distribution was demonstrated by N–CN through the N_2 adsorption-desorption isotherms (figure 9(b)), leading to a BET specific surface area (348.17 m^2 g^{-1}) that is almost 13 times larger than CN to provide more loading sites. Owing to the strong electronic interaction between IrO_2 and N–CN, IrO_2/N–CN presented the optimal OER potential of 1.778 V and good durability for 300 h at current density of 1.6 A cm^{-2}. Furthermore, theoretical calculations revealed the superiority of IrO_2/N–CN in OER kinetics and indicated that the energy barrier of the RDS of IrO_2/CN ($^*OH \rightarrow {}^*O$, 1.42 eV) could be reduced in IrO_2/N–CN (figure 9(c)). The density of state profile further verified the formation of Ir–N bonds and strong electronic interaction in IrO_2/N–CN from a larger overlap between occupied N p orbitals and Ir d orbitals, contributing to weakened adsorption of oxygen intermediates to improve the overall kinetics.

Recent studies have demonstrated that stabilizing the Ir-based catalyst on the one-dimensional (1D) rather than 2D nanomaterial supports is also viable in boosting the electrochemical performance [150]. The allure of 1D nanomaterials is from the increased surface area for more loading sites, the abundance of open spaces among the adjacent 1D nanomaterials to promote mass accessibility, and efficient oriented charge transport [151]. For instance, Jiang *et al* designed an ordered array nanostructured electrode with defective Ir

film coated on WO_x nanorods support (Ir@WO_xNRs) [152]. WO_x nanorods were grown on W foil through hydrothermal synthesis and Ir catalyst was electrodeposited on the surfaces of WO_xNRs, followed by preparation of MEA via decal transfer process (figure 10(a)). By increasing CV deposition to 100 cycles, significant aggregation of Ir led to the formation of a defective Ir film (figure 10(b)). The optimal Ir coating (Ir@WO_xNRs-100) had a mass loading of 0.14 mg_{Ir} cm^{-2} to obtain a better performance of 2.2 A cm^{-2} at 2.0 V and brilliant stability of 1030 h at 0.5 A cm^{-2}, superior to that of commercial Ir black CCM. Not only could the WO_x support with appropriate porosity and ordered nanorod nanostructure stabilize the dispersion of Ir and provide vertical electron transport channels, but it also promoted water conservation and transportation. In addition, 1D nanostructures can strengthen the interaction between the particles in the CL. Hegge *et al* designed a hybrid structure combining IrO_x nanofibers with a conventional IrO_x nanoparticles CL and successfully reduced the Ir loading to 0.2 mg_{Ir} cm^{-2}, exceeding the performance of MEAs with anodes of only either IrO_x nanofibers or IrO_x nanoparticles [153]. The IrO_x nanofibers interlayers formed a good electrical connection throughout the region and facilitated the distribution of electrons over the CL, strengthening the connectivity of the particles instead of leaving electrically disconnected regions in the CL with only nanoparticles (figures 10(c) and (d)). This was also evidenced by in-plane conductivity due to the obviously lower sheet resistance for the hybrid CL, compared with the non-hybrid counterparts with the same IrO_x loading. Although the 1D support exhibits superiority in various aspects, the density and morphology of the nanostructure should also be taken note of to avoid overloading. Hrbek *et al* reported a fiber-like structure of a CeO_x layer serving as catalyst support in a PEMWE, which was deposited on PEM through reactive magnetron sputtering to form CCM, together with simultaneous plasma etching of the PEM [154]. The working pressure during the treatment was optimized at 0.4 Pa, balancing between the level of structural porosity and avoiding fiber shortening and densification at high pressure that would disrupt the electron pathway and cause poor dispersion. The optimized support with could efficiently stabilize a thin-film Ir catalyst, with combined Pt + Ir loading of 220 μg cm^{-2}.

4.2.2. Catalyst materials

It is worth noting that the oxidation state of Ir can correlate with the OER activity. For example, Kim *et al* successfully loaded the Ir catalyst onto a highly roughened dendritic Au support grown on a CP substrate, and the Ir metal loading was controlled at a microgram scale (Ir/Au/CP) by the number of Ir electrochemical deposition pulse [155]. With increasing Ir coverage, the Ir $4f_{7/2}$ peak binding energy and $Ir^{3+} + Ir^{4+} + Ir^{>4+}$ peak area ratio continuously declined (figure 11(a)) due to the increased surface density of the Ir–Au interface and the presence of electron density gradient throughout Ir islands in the direction normal to the Ir–Au interface in view of electronic depletion at the Ir–Au interface. In addition, the optimal Ir-based GDE (30Ir/Au/CP, where the number of deposition pulse is 30) was EC and thermally (TC) oxidized to change the Ir electronic structure by forming IrO_x, aiming at adjusting the balance between activity and stability. The relationship between specific activity and $Ir^{3+}/(Ir^{3+} + Ir^{4+})$ ratio was thereupon established (figure 11(b)), further demonstrating the influence of the oxidation state of Ir on OER activity, which decreases in the order of EC-IrO_x/Au/CP > 30Ir/Au/CP > TC-IrO_x/Au/CP. With lower contribution from ohmic overpotential and mass-transfer losses even in the high current density region (figure 11(c)), a high Ir mass activity of 440.5 A mg_{Ir}^{-1} at 1.9 V was achieved using 30Ir/Au/CP. Besides, Cha *et al* discovered the relationship between the surface oxidation of Ir and the dissolution rate by investigating IrO_x/Ti_4O_7 catalyst with various iridium/support ratios [156]. With a higher $Ir^{4+}/[Ir^{3+} + Ir^{4+}]$ ratio, less iridium degradation was observed under OER conditions, suggesting better corrosion resistance and good stability. A similar conclusion was also drawn by Saveleva *et al*, where a diminution in Ir dissolution rate and slower establishment of a steady state were observed in oxidized Ir nanoparticles supported on Sb-doped SnO_2 aerogel compared with the unsupported catalyst [157]. This could be attributed to the decrease in the formation of highly unstable Ir^{3+} since the dissolution process tended to occur through the formation of intermediates in the oxidation state Ir^{3+}. At this point, it can be summarized that a trade-off of Ir^{3+} and Ir^{4+} can enhance the intrinsic OER activity and stability.

Modifications focusing on the OER catalyst itself is also an indispensable part of boosting its performance in MEA. Strategies employed to regulate the structure-performance relationship of noble-metal-based catalysts include defect engineering, strain engineering, and hybrid engineering [158]. Huang *et al* utilized Co-hexamethylenetetramine metal–organic framework as the precursor and a fast-quenching method to synthesize tensile-strained RuO_2 nanorods growing on antimony-tin oxide (ATO) particles (s-RuO_2/ATO) [35]. The tensile strain induced by the fast-quenching process altered the electronic state of RuO_2. The x-ray diffraction peaks of s-RuO_2 revealed the expanded lattice parameters relative to the normal RuO_2, exhibiting the tensile strains within the nanorods. Moreover, in the Fourier-transformed extended x-ray absorption fine structure (FT-EXAFS) (figure 11(d)), the longer radial distance was observed for the first and second shells of s-RuO_2/ATO than that of n-RuO_2/ATO (without quenching process). Besides, a shift of E_g peak of

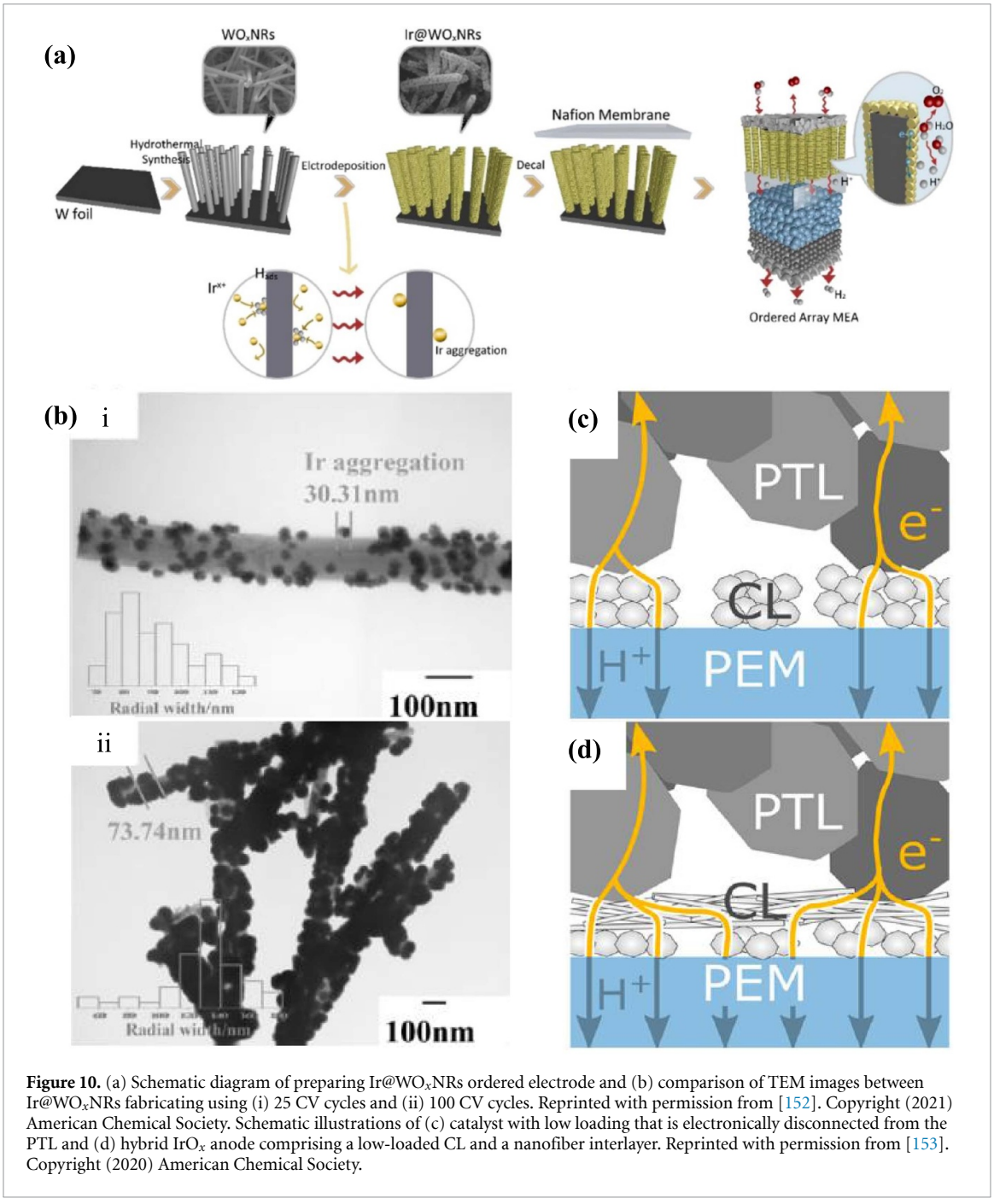

Figure 10. (a) Schematic diagram of preparing Ir@WO_xNRs ordered electrode and (b) comparison of TEM images between Ir@WO_xNRs fabricating using (i) 25 CV cycles and (ii) 100 CV cycles. Reprinted with permission from [152]. Copyright (2021) American Chemical Society. Schematic illustrations of (c) catalyst with low loading that is electronically disconnected from the PTL and (d) hybrid IrO_x anode comprising a low-loaded CL and a nanofiber interlayer. Reprinted with permission from [153]. Copyright (2020) American Chemical Society.

s-RuO_2/ATO to a lower wavenumber in the Raman spectrum (figure 11(e)) further verified the presence of tensile strain. As a result, the energy barrier of the limiting step of OER was reduced and the absorption energies of oxygen intermediates were also weakened on the tensile-strained RuO_2 (figures 11(f) and (g)). Impressively, the resultant PEMWE required only 1.51 V to reach a current density of 1 A cm^{-2}.

Another modification strategy is constructing a composite catalyst such as IrO_2–RuO_2 composites. The durability of IrO_2 exceeds that of RuO_2 while RuO_2 has higher OER activity, thus combining these two components can obtain a highly robust OER catalyst in the MEA anode but the resulting MEA is still costly [159, 160]. Nevertheless, the cost of the MEA can be reduced when noble-metal-free components are used to dilute the content of noble metal in composite electrocatalysts [161]. For instance, Kaya *et al* investigated the magnetized IrO_2–Fe_3O_4 as an anode catalyst in MEA that exhibited a four-fold increase in MEA current

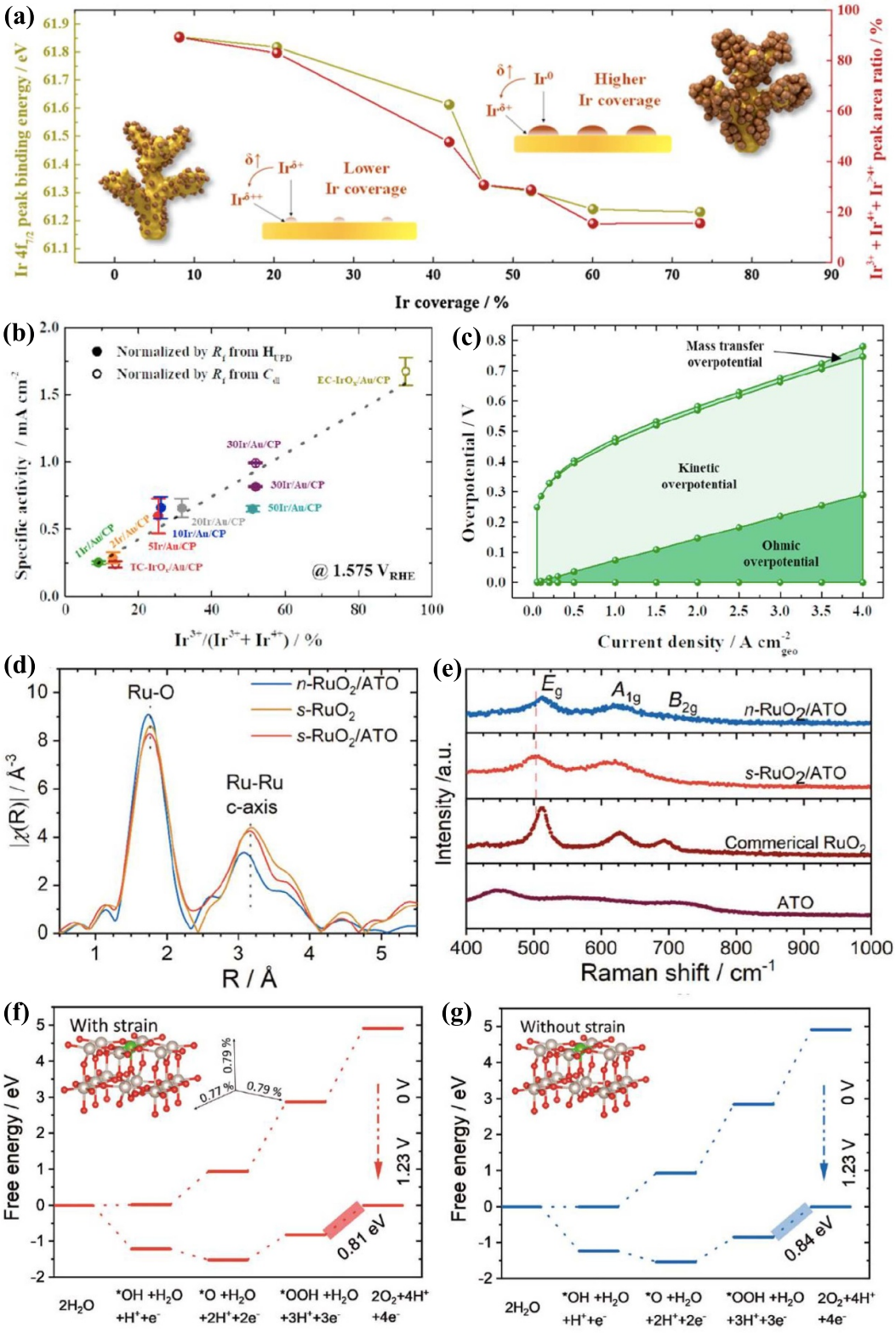

Figure 11. (a) Ir $4f_{7/2}$ peak binding energy and $Ir^{3+} + Ir^{4+} + Ir^{>4+}$ peak area ratio as functions of Ir coverage, (b) the relationship between specific activity and $Ir^{3+}/(Ir^{3+} + Ir^{4+})$ ratio, and (c) overpotential subdivisions of cell overpotential based on PEMWE polarization curve in a single cell comprising 30Ir/Au/CP anode. Reprinted from [155], Copyright (2020), with permission from Elsevier. (d) The Ru K-edge FT-EXAFS spectra of n-RuO_2/ATO, s-RuO_2, and s-RuO_2/ATO after phase corrections, (e) the Raman spectra of n-RuO_2/ATO, s-RuO_2/ATO, commercial RuO_2, and ATO, and the free energy diagrams of (f) s-RuO_2 and (g) RuO_2 calculated on the coordinatively unsaturated sites. Reproduced from [35]. CC BY 4.0. © 2022 The Authors. Advanced Science published by Wiley-VCH GmbH.

density in comparison with the non-magnetized and pristine IrO_2 catalyst. The loading of IrO_2 was significantly reduced in the composite CL by replacing 20% of IrO_2 with the more abundant and cheaper Fe_3O_4 while retaining high electrochemical performance [162]. Moreover, a ternary composite can be constructed to take the advantage of the synergy between more components. By applying IrO_2–RuO_2–TaO_x coating on Ti felts PTL via a thermal deposition method, the precious metal loading was decreased to 1 mg cm^{-2} and achieved a performance of 1.836 V at 2 A cm^{-2} in a single cell, owing to combination of the high stability of IrO_2 and TaO_x in the acidic environment and the high OER catalytic activity of RuO_2 [163].

OER activity of a catalyst can also be optimized by tuning its morphology or architecture. The morphology-controlled nanostructures are able to provide an unsaturated coordination environment for a more reactive reaction [164]. For example, Park *et al* fabricated an IrO_2 inverse-opal MEA as an anode for OER via the decal-transfer method [165]. The inverse-opal structure was synthesized by utilizing self-assembled polystyrene (PS) beads on a Ni-sputtered fluorine-doped tin oxide substrate. Thereinto, PS was utilized as a template to construct micropores in the electrode, followed by infiltration of IrO_2 through pulse electrodeposition while adjusting the number of cycles to attain the optimal structure (with the optimal number of cycles being 140 k) with high porosity (figures 12(a) and (b)). By reducing the catalyst loading to 0.02 mg cm^{-2}, inverse-opal MEA outperformed the conventional MEA by delivering 870 mA cm^{-2} at 1.6 V, which is 2.5 times that of the latter. Also, there was no decline in the performance of the novel MEA with micro-pores in the high-voltage region (while it was obvious for the conventional MEA) due to promoted mass transport for reactants and products, which mitigated active site blockage. Besides, the novel MEA had lower ohmic resistance and charge-transfer resistance due to the ordered and interconnected pores to promote charge transfer.

In addition, another way to beneficially modify the architecture of the catalyst is by synthesizing core–shell catalysts with unique physical and chemical properties. Several advantages can be obtained from a core–shell structure, including introduction of interfacial strain that tunes the electronic structure, modified atomic vicinity that affects the charge transfer, increased surface area, providing protection to the unstable core by isolating it from the external environment, and facilitating the full utilization of the surface material [166, 167]. On this ground, the core–shell structure is expected to effectively regulate the intrinsic catalytic activity and stability of the resultant material, simultaneously lowering the noble metal loading. For example, Zheng *et al* synthesized a core–shell electrocatalyst with an $IrRu_x$ core and Ir-rich shell ($IrRu_x$@Ir) via a CO-induced phase-segregation strategy [168]. The electronic interaction between the core and the shell induced efficient charge transfer from Ir to $IrRu_x$, thus tuning the electronic structure of the shell and increasing the oxidation state of surface Ir sites to improve the OER activity. The Ir shell protected the inner Ru atom against the dissolution and retained the structural stability during the durability test in the acidic environment. Similarly, Lv *et al* designed a self-assembled RuO_2@IrO_x core–shell heterostructure nanocomposite, in which the Ir-based shell also effectively protected the RuO_2 core from dissolution, resulting in a cell potential of 1.683 V at 1 A cm^{-2} and with enhanced catalyst durability [36]. In-depth exploration of the core–shell structure further shows its promise in producing stable catalyst ink, which is often the most overlooked parameter for fabrication of large-area electrodes with homogeneous catalyst deposition. Pham *et al* synthesized IrO_2-coated TiO_2 core–shell microparticles (IrO_2@TiO_2) as an OER catalyst, and deposited them on Ti PTL [169]. There were two steps in the synthesis process based on surface charge modification indicated by zeta potentials of TiO_2 particle in ethanol solution (figure 12(c)): (1) formation of H_2IrCl_6 shell on TiO_2 core, which depended on the surface charge of TiO_2 that was converted from negative to positive by adding acetic acid and H_2IrCl_6 for better attachment of $[IrCl_6]^{2-}$ anions, followed by continuously growing H_2IrCl_6 shells around the TiO_2 particles upon solvent evaporation; and (2) conversion of H_2IrCl_6 shell into an IrO_2 layer via pyrolysis at 500 °C for 30 min in air. The stability of the catalyst ink was reflected in back-scattering signal intensity that was influenced by the ink destabilization (figure 12(d)). The back-scattering signal intensity of IrO_2@TiO_2 was relatively even throughout the height of the ink compared with that of mixed IrO_2 + TiO_2 powders that would have undergone sedimentation, manifesting the high stability of IrO_2@TiO_2 ink due to surface changes by IrO_2 coverage.

Impressively, competitive durability of the OER catalyst could be achieved even with low-iridium PEMWE MEA. Möckl *et al* investigated the durability of a novel iridium catalyst with a low iridium packing density (derived from amorphous hydrous iridium oxide deposited as thin film on low surface area TiO_2) in a ten-cell water electrolyzer short stack, where the first five cells utilized conventional catalyst with iridium loading of 2 mg_{Ir} cm^{-2} and the last five cells applied the novel catalyst with a lower loading of 0.25 mg_{Ir} cm^{-2} [170]. The MEA was tested for 3700 h under ambient pressure and 60 °C by load current density cycling between 0.2, 1.0, and 2.0 A cm^{-2}. Although the low-loading catalyst exhibited 30-fold higher beginning-of-life mass-activity, there was a pronounced rise in the cell voltage during the first 1000 h for stabilization, but less significant during the rest of the time for both types of catalysts. This was attributed to the change in the oxidation state of the catalyst surface as it converts into the less active IrO_2. Similar

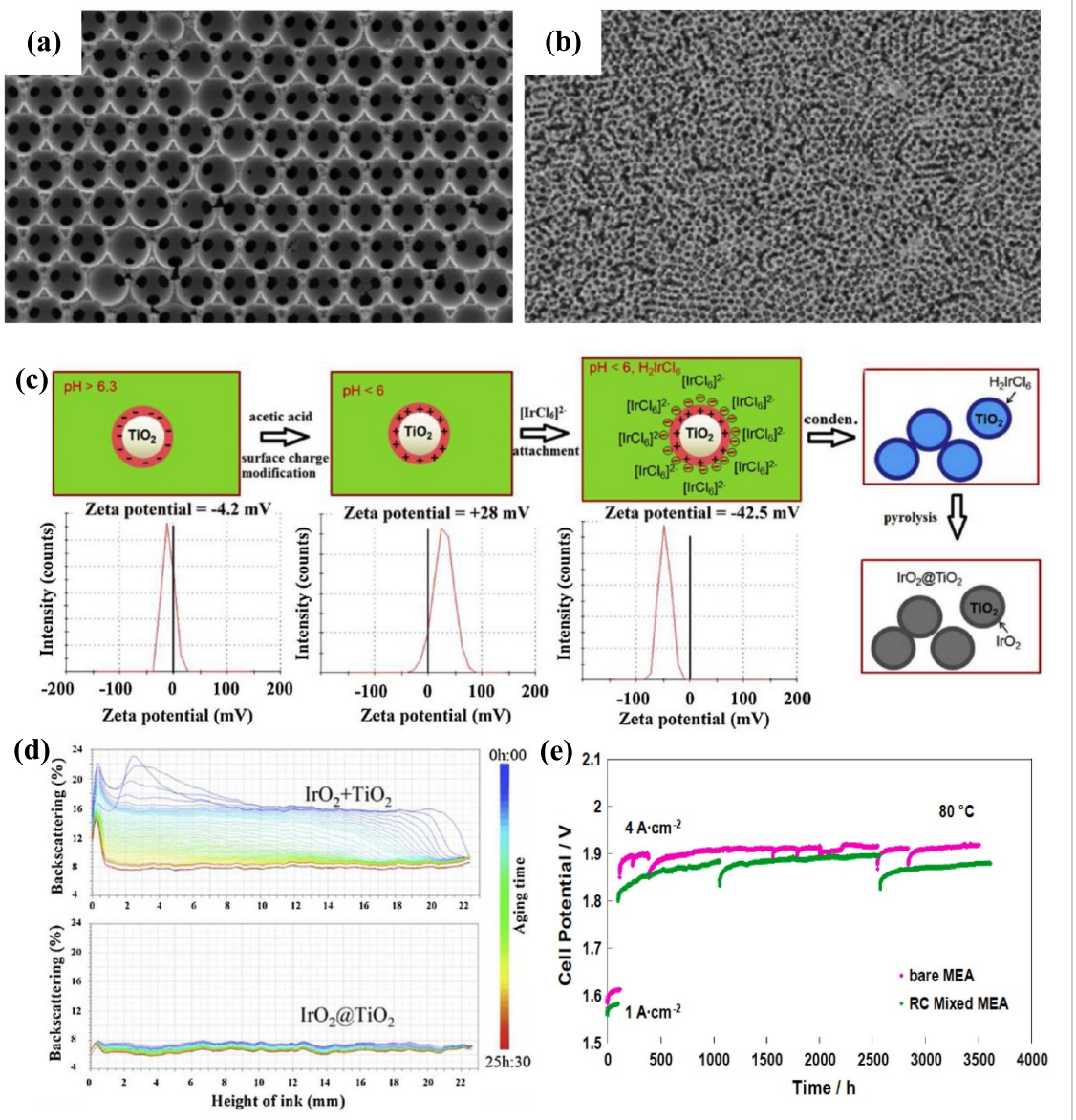

Figure 12. (a) FE-SEM images of the inverse-opal electrode with the scale bar of 1 μm and (b) inverse-opal electrode with the scale bar of 5 μm, obtained when the total number of cycles is 140 k. Reprinted from [165], Copyright (2019), with permission from Elsevier. (c) Schematic illustration of synthesizing IrO_2@TiO_2 catalyst, in which the surface charge was manifested in zeta potential of the particle in ethanol solution, and (d) the ink stability test of IrO_2@TiO_2 and IrO_2 + TiO_2 catalyst based on the evolution of backscattering spectra. Reproduced with permission from [169]. © 2020 The Authors. Published by Elsevier B.V. (e) Durability test at 1 and 4 A cm^{-2} under 80 °C for bare and integrated PtCo catalyst-based MEAs. Reprinted from [171], Copyright (2020), with permission from Elsevier.

durability trend was observed by Pantò *et al* on an MEA with recombination catalyst-based anode ($IrRuO_x$ + PtCo) and Pt/C cathode that enabled an even lower PGM loading of 0.6 mg_{MEA} PGM cm^{-2} [171]. The test was carried out for 3500 h, with 100 h at 1 A cm^{-2} and 3400 h at 4 A cm^{-2} (figure 12(e)), and the cell voltage was found to have increased rapidly at the beginning, which was ascribed to the accumulation of the gases in the micropores of catalysts in addition to the modification of the oxidation state at the anode catalyst surface. During the test, the novel MEA exhibited lower degradation and delivered a cell voltage that was 30 mV lower than that without PtCo (bare MEA), thus successfully reaching a voltage efficiency of ~80% at 4 A cm^{-2}.

Summarily, most studies are still focused on optimizing noble metal catalyst (RuO_2 and IrO_2) to achieve high OER activity at the anode of a MEA, since they are highly active and acid-durable OER catalysts. As they are precious metals, their scarcity and high material cost will inhibit widespread PEMWE adoption. Therefore, great efforts have been devoted to developing appropriate support materials to minimize the loading of precious metals in the electrode while retaining the electrochemical performance of the current commercial OER catalysts (table 2). Future exploration on novel catalysts to replace the utilization of noble metal-based OER catalysts in PEMWE MEA is necessary.

Table 2. Representative summary of OER anode catalysts in MEA.

Anode catalyst	Fabrication method	GDL/PTL	Membrane	Electrochemical performance	Catalyst/noble metal loading	Stability	References
IrO_x/Ti_4O_7(7:3)	GDE	Pt-coated Ti PTLs	Nafion 115	1.54 V@1 A cm^{-2} 1.64 V@2 A cm^{-2}	0.961 mg cm^{-2} (13.5 Ir wt%)	>50 h@1 A cm^{-2}	[156]
Ir@WO_xNRs	CCM	Pt-coated Ti PTLs	Nafion115	2.2 A cm^{-2}@2.0 V	0.14 mg_{Ir} cm^{-2}	>1030 h@0.5 A cm^{-2}	[152]
Ir–Pt–TiO_2–PC-ann	CCM	Ti PTLs	Nafion 117	1.87 V@1 A cm^{-2}	1.0 mg_{pgm} cm^{-2}	N/A	[142]
30Ir/Au/CP	GDE	CP	Nafion 212	1.652 V@1 A cm^{-2} 1.758 V@2 A cm^{-2}	0.008 mg_{Ir} cm^{-2}	20 h for each sequential 0.10, 0.25, and 0.50 A cm^{-2}	[155]
IrO_2/TNO	CCM	CP	Nafion 117	1.832 V@1 A cm^{-2}	2.5 mg_{Ir} cm^{-2}	>100 h@1 A cm^{-2}	[144]
Ir–CeO_x (0.4 Pa anode-CCM)	CCM	Pt-coated micro grained Ti GDL	Nafion NE 1035	3.18 A cm^{-2}@1.9 V	113 mg_{Ir} cm^{-2}	N/A	[154]
$IrRuO_x$	CCM	Titanium fiber mesh	Aquivion membrane (E98-05S, with thickness of 50 μm)	4 A cm^{-2}@1.86 V 8 A cm^{-2}@2.15 V	0.3 mg_{Ir+Ru} cm^{-2}	>3500 h@4 A cm^{-2}	[171]
$Ru_{0.8}Pd_{0.2}O_2$	CCM	N/A	Nafion 115	2.03 V@1 A cm^{-2}	3.0 mg cm^{-2}	>100 h@1 A cm^{-2}	[161]
$IrRu_x$@Ir	CCM	N/A	Nafion 115	N/A	1.5 mg cm^{-2}	>400 h@1 A cm^{-2}	[168]
s-RuO_2/ATO	CCM	N/A	Nafion 212	1.51 V@1 A cm^{-2}	3.3 mg cm^{-2} (19.4 Ru wt%)	>40 h@0.5 A cm^{-2}	[35]
IrO_2/N–CN	CCM	Porous sintered titanium plate	Nafion 117	1.778 V@1.6 A cm^{-2}	1.5 mg cm^{-2} for IrO_2	>300 h@1.6 A cm^{-2}	[149]
RuO_2@IrO_x	CCM	Porous titanium mesh	Nafion 117	1.683 V@1 A cm^{-2}	2.5 mg cm^{-2}	>300 h@1 A cm^{-2}	[36]
80%IrO_2–20%Fe_3O_4	CCM	Pt coated Ti mesh	Nafion 115	2.42 V@1 A cm^{-2}	3 mg cm^{-2}	N/A	[162]
IrO_2@TiO_2	GDE	Fiber sintered titanium substrates	Nafion 212	1.67 V@1 A cm^{-2}	0.4 mg_{Ir} cm^{-2}	>150 h@2 A cm^{-2} for IrO_2@TiO_2 with 0.5 mg_{Ir} cm^{-2}	[169]
IrO_2 inverse-opal electrode	CCM	Carbon-based GDL	Nafion 212	870 mA cm^{-2}@1.6 V	0.02 mg cm^{-2} (10 wt% IrO_2)	1.6 V and 1.9 V for a period of 1200 s	[165]
$(M,Ru)O_2$ (M = Mg, Zn, Cu, Ni, Co) rutiles	CCM	CP	Nafion 117	1.383 V@1 mA cm^{-2} for $(Cu,Ru)O_2$	PGM loading between 0.05 and 0.15 mg cm^{-2}	1500 cycles at 0.6−1.35 V vs RHE at 100 mV s^{-1}	[172]
IrO_2–RuO_2–TaO_x	CCM	Ti felt	Nafion 115	1.836 V@2 A cm^{-2}	1 mg cm^{-2} Ir	N/A	[163]
IrO_x hybrid (IrO_x nanofiber interlayer on IrO_x nanoparticles)	CCM	Sintered titanium fiber PTL	Nafion 115/212	1.69 V@2 A cm^{-2} for Nafion 212	0.2 mg_{Ir} cm^{-2}	>150 h@2 A cm^{-2} for Nafion 115	[153]
Ir AC/NN	CCM	Ti felt	Nafion 212	1.82 V@3 A cm^{-2}	1.0 mg cm^{-2}	>90 h@3 A cm^{-2}	[150]
20% IrO_x/30% W-TiO_2	CCM	N/A	Nafion 212	1.602 V@1 A cm^{-2}	0.116 mg cm^{-2} IrO_x	>400 h@1 A cm^{-2}	[143]
$Ir_{0.7}Ru_{0.3}O_2$	CCM	N/A	Nafion 115	1.656 V@1 A cm^{-2}	1.8 mg cm^{-2}	4 h@0.2 A cm^{-2} for conditioning, followed by 1 A cm^{-2} for 44 h	[34]

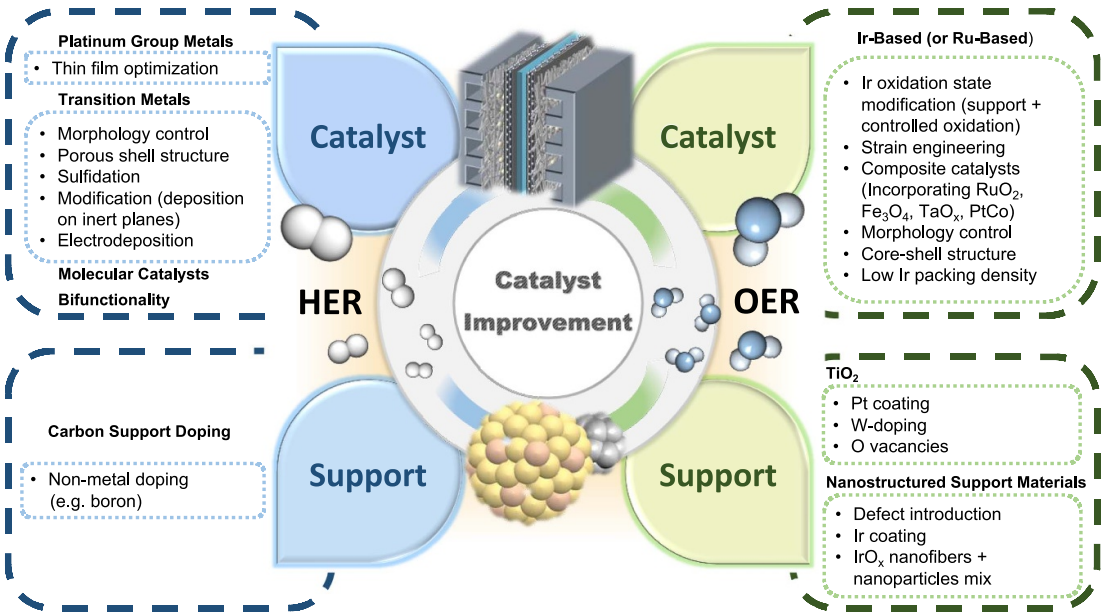

Figure 13. An overview of catalyst improvement works discussed in this review.

5. Conclusion and perspectives

Water electrolysis is the most suitable technology to produce hydrogen sustainably without producing any undesirable by-products. To drive the industrial development of water electrolysis further, scientists are seeking a way to improve the catalysts and the membranes as well as their integration into MEA, the core of a water electrolyzer. An electrolyzer utilizing PEM in MEA produces an acidic environment for hydrogen production. Compared with other commercially available electrolyzers, PEMWE can usually present higher performance, but the cost and the corrosive reaction environment are inhibiting its widespread commercial adoption.

To discuss PEMWE and its challenges in detail, different fabrication methods to incorporate electrocatalysts into MEA have been first introduced in this review, whereby CCM and CCE are the most common approaches that have potentials for industrial application. The importance of facilitating favorable catalyst-membrane interaction through the fabrication process has been highlighted. The innovative modification strategies applied to electrodes and membranes to ameliorate the performance of PEMWE have been discussed, focusing on efforts to improve charge and mass transport efficiencies and improving the lifetime of the membranes. In addition, recent encouraging progress in the development of HER and OER catalysts, summarized in figure 13, has been reviewed to provide a better comprehension on rational design of high-performance catalysts used in MEAs. In particular, various synthesis strategies to produce thin films of Pt catalysts and replacing Pt have been the focus of studies on HER catalysis, whereas OER catalysis studies are dominated by the improvement of catalyst supports and the structural modification of precious-metal-based catalysts.

Despite the brilliant achievements in PEMWE, there are still challenges to be addressed. Firstly, in addition to the innovative and facile synthesis methods developed to improve the device performance and manufacturability, the environmentally friendly synthesis methods designed for environmental sustainability are easily overlooked. Green chemistry plays a pivotal role in environmental management, whereby the chemical process is designed in a way that reduces or eliminates the use or generation of hazardous materials, thus speeding up the progress toward sustainable development goals [173, 174]. As mentioned, precious-metal-based electrocatalysts, especially those containing Ir, are still widely used for OER anode in PEMWE. Common catalyst synthesis methods such as hydrothermal method, electrodeposition, and sol–gel method lack both good morphology control and environmental sustainability. Therefore, it would be rewarding to explore ways that fulfill both these requirements. Faustini *et al* prepared an Ir-containing oxide anode catalyst ($Ir_{0.7}Ru_{0.3}O_2$) with a hierarchical ultraporous architecture comprising a nanoneedle network assembled into microporous micrometric particles, which enabled high accessibility of reactants to the catalytically active surface during PEMWE operation [34]. They also proposed a spray-drying fabrication process using water as a solvent to assist the evaporation-induced self-assembly, which is cost-effective,

waste-free, and easily scalable. This approach conferred both the ability to tune the chemical composition of the catalysts and the ability to introduce porosity using templates.

Secondly, to accommodate the industrial operation, a PEMWE should be able to withstand the harsh conditions of high current density and high pressure in order to reduce operational cost [11]. Although many papers have claimed the high performance of their PEMWE catalysts at ampere-level (1–4 A cm^{-2}), it is still difficult to compare the performance of a single cell with other reported systems since the parameters in other electrolyzers may be different, such as testing condition (e.g. different current densities), membrane type, and catalyst mass loading. A few studies introduced the Ir-mass-normalized power density metric (which is obtained by dividing the cell power density by noble metal loading) to eliminate the influence of other testing factors with a focus on catalyst utilization [103, 169]. Besides, the deviation also lies in the geometrical area of the working electrode used to normalize the current density because it differs from the actual catalytic surface area. Hence, it is necessary to establish a series of standardized criteria for comparing the performance of MEAs for water electrolysis.

Thirdly, the majority of the studies have dived into developing efficient electrodes and optimizing the operating parameters, which can deliver minimal overpotential and consume less power at near industrial-scale current density by the experimental practices. On one hand, developing advanced PEMs, GDLs, and electrocatalysts will continue to be the hotspot of future research, which will place emphasis on the cost and lifetime of their materials, accompanied by specific requirements for the reduced gas permeability of PEM, sufficiently robust coating of GDL, and highly catalytic activity of electrocatalysts. On the other hand, optimization done by experimental approaches is challenging from the viewpoints of cost, time, and technical restrictions. As such, involving artificial intelligence and data science in PEMWE development for comprehensive investigation is desirable for accurately optimizing electrolyzer design and predicting the best structure of potential catalysts based on algorithms. For example, machine learning can guide the design of a PEMWE electrolyzer by fast and easy simulation of the hydrogen production rate and cell current density of the electrolyzer by correlating with various design parameters to obtain the optimal result to guide the subsequent experiments [175]. Hence, assistance by machine learning offers the best approach to achieving high performance at the shortest possible time.

With the help of advance manufacturing technologies, more efficient fabrication of electrolyzers can be realized. Three-dimensional (3D) printing, the well-known subset of additive manufacturing, is the most widely used technology for expeditious prototyping through layer-by-layer fabrication of an object based on its 3D model data [176]. Therefore, it offers flexibility to produce microscale structures in a programmable and facile fashion, with a well-controlled design in shape, size, and porosity [177]. Ignited by this technology, 3D-printable MEA becomes appealing. To our delight, some studies have demonstrated the successful application of 3D printing technology to manufacture the components in MEA [178]. For example, Yang *et al* fabricated 3D-printable bipolar plates using fused deposition modeling without any post-processing, which provided a rapid synthesis route for the mechanical support of the electrolyzer [179]. Besides, 3D printing is also useful in fabricating heterogeneous catalysts, especially for industrial catalysts. For instance, robocasting can be used to fabricate structured monoliths and powder bed 3D printing methods can be explored to produce catalysts of various shapes [180, 181]. Hence, the emerging 3D printing technology showcases its potential in MEA manufacturing for water electrolysis in a more precise and efficient manner while retaining the overall cell performance.

Finally, a good MEA is a kernel of realizing the high efficiency of electrolytic cells industrially, which is the unremitting pursuit of researchers. Hence, the collaboration between industry and academia to improve the performance and encourage widespread adoption of the state-of-the-art PEMWE technology is crucial. In improving industrial water electrolysis, multidisciplinary cooperation between engineering and sciences can provide farsighted solutions.

Data availability statement

The data that support the findings of this study are available upon reasonable request from the authors.

Acknowledgments

This work is supported by the Singapore Ministry of Education (MOE) Tier 1 Grant (RG62/21), MOE Tier 2 Grant (MOE-T2EP10220-0001) and A*STAR (Agency for Science, Technology and Research) under its LCERFI program (Award No. U2102d2002).

Conflict of interest

There are no conflicts to declare.

ORCID iDs

Justin Zhu Yeow Seow https://orcid.org/0000-0002-0904-6844
Zhichuan J Xu https://orcid.org/0000-0001-7746-5920

References

[1] Li L, Wang P, Shao Q and Huang X 2021 Recent progress in advanced electrocatalyst design for acidic oxygen evolution reaction *Adv. Mater.* **33** 2004243
[2] Zhao G, Kraglund M R, Frandsen H L, Wulff A C, Jensen S H, Chen M and Graves C R 2020 Life cycle assessment of H_2O electrolysis technologies *Int. J. Hydrog. Energy* **45** 23765–81
[3] Xu Q, Zhang L, Zhang J, Wang J, Hu Y, Jiang H and Li C 2022 Anion exchange membrane water electrolyzer: electrode design, lab-scaled testing system and performance evaluation *EnergyChem* **4** 100087
[4] Bareiß K, de la Rua C, Möckl M and Hamacher T 2019 Life cycle assessment of hydrogen from proton exchange membrane water electrolysis in future energy systems *Appl. Energy* **237** 862–72
[5] Andrews J W 2020 Hydrogen production and carbon sequestration by steam methane reforming and fracking with carbon dioxide *Int. J. Hydrog. Energy* **45** 9279–84
[6] Brandon N P and Kurban Z 2017 Clean energy and the hydrogen economy *Phil. Trans. R. Soc.* A **375** 20160400
[7] Yan X L and Hino R 2011 *Nuclear Hydrogen Production* (Boca Raton, FL: CRC Press) pp 47–80
[8] Zhao G, Rui K, Dou S X and Sun W 2018 Heterostructures for electrochemical hydrogen evolution reaction: a review *Adv. Funct. Mater.* **28** 1803291
[9] Jin H, Wang J, Su D, Wei Z, Pang Z and Wang Y 2015 *In situ* cobalt–cobalt oxide/N-doped carbon hybrids as superior bifunctional electrocatalysts for hydrogen and oxygen evolution *J. Am. Chem. Soc.* **137** 2688–94
[10] Buttler A and Spliethoff H 2018 Current status of water electrolysis for energy storage, grid balancing and sector coupling via power-to-gas and power-to-liquids: a review *Renew. Sustain. Energy Rev.* **82** 2440–54
[11] Babic U, Suermann M, Büchi F N, Gubler L and Schmidt T J 2017 Critical review—identifying critical gaps for polymer electrolyte water electrolysis development *J. Electrochem. Soc.* **164** F387–F99
[12] Wang T, Cao X and Jiao L 2022 PEM water electrolysis for hydrogen production: fundamentals, advances, and prospects *Carbon Neutrality* **1** 21
[13] Paidar M, Fateev V and Bouzek K 2016 Membrane electrolysis—history, current status and perspective *Electrochim. Acta* **209** 737–56
[14] Frydendal R, Paoli E A, Chorkendorff I, Rossmeisl J and Stephens I E L 2015 Toward an active and stable catalyst for oxygen evolution in acidic media: Ti-stabilized MnO_2 *Adv. Energy Mater.* **5** 1500991
[15] Xu X, Sun H, Jiang S P and Shao Z 2021 Modulating metal–organic frameworks for catalyzing acidic oxygen evolution for proton exchange membrane water electrolysis *SusMat* **1** 460–81
[16] Liu L 2021 Platinum group metal free nano-catalysts for proton exchange membrane water electrolysis *Curr. Opin. Chem. Eng.* **34** 100743
[17] Zhang K and Zou R 2021 Advanced transition metal-based OER electrocatalysts: current status, opportunities, and challenges *Small* **17** 2100129
[18] Fu Q *et al* 2021 2D transition metal dichalcogenides: design, modulation, and challenges in electrocatalysis *Adv. Mater.* **33** 1907818
[19] Song J, Wei C, Huang Z-F, Liu C, Zeng L, Wang X and Xu Z J 2020 A review on fundamentals for designing oxygen evolution electrocatalysts *Chem. Soc. Rev.* **49** 2196–214
[20] Zhou L, Lu S-Y and Guo S 2021 Recent progress on precious metal single atom materials for water splitting catalysis *SusMat* **1** 194–210
[21] Romiluyi O, Danilovic N, Bell A T and Weber A Z 2023 Membrane-electrode assembly design parameters for optimal CO_2 reduction *Electrochem. Sci. Adv.* **3** e2100186
[22] Kopljar D, Inan A, Vindayer P, Scholz R, Frangos N, Wagner N and Klemm E 2015 Development and utilization of gas diffusion electrodes for the electrochemical reduction of CO_2 *Chem. Ing. Tech.* **87** 855–9
[23] Weng L-C, Bell A T and Weber A Z 2018 Modeling gas-diffusion electrodes for CO_2 reduction *Phys. Chem. Chem. Phys.* **20** 16973–84
[24] Wang G, Zou L, Huang Q, Zou Z and Yang H 2019 Multidimensional nanostructured membrane electrode assemblies for proton exchange membrane fuel cell applications *J. Mater. Chem.* A **7** 9447–77
[25] Kulkarni N, Kok M D R, Jervis R, Iacoviello F, Meyer Q, Shearing P R and Brett D J L 2019 The effect of non-uniform compression and flow-field arrangements on membrane electrode assemblies—x-ray computed tomography characterisation and effective parameter determination *J. Power Sources* **426** 97–110
[26] Chatenet M *et al* 2022 Water electrolysis: from textbook knowledge to the latest scientific strategies and industrial developments *Chem. Soc. Rev.* **51** 4583–762
[27] Ionescu V 2020 Water and hydrogen transport modelling through the membrane-electrode assembly of a PEM fuel cell *Phys. Scr.* **95** 034006
[28] Bhosale A C, Ghosh P C and Assaud L 2020 Preparation methods of membrane electrode assemblies for proton exchange membrane fuel cells and unitized regenerative fuel cells: a review *Renew. Sustain. Energy Rev.* **133** 110286
[29] Zhang K *et al* 2022 Status and perspectives of key materials for PEM electrolyzer *Nano Res. Energy* **1** e9120032
[30] Wang X L, Qu Z G, Lai T, Ren G F and Wang W K 2022 Enhancing water transport performance of gas diffusion layers through coupling manipulation of pore structure and hydrophobicity *J. Power Sources* **525** 231121

[31] Mehrpooya M, Nouri G, Eikani M H, Khandan N and Hajinezhad A 2016 Effects of membrane electrode assembly fabrication parameters on the proton exchange membrane fuel cell performance *Int. J. Ambient Energy* **37** 639–44
[32] Zahiri B, Felix R M, Hill A, Kung C H, Sharma T, Real J D and Mérida W 2018 Through-plane wettability tuning of fibrous carbon layers via O_2 plasma treatment for enhanced water management *Appl. Surf. Sci.* **458** 32–42
[33] Omrani R and Shabani B 2017 Gas diffusion layer modifications and treatments for improving the performance of proton exchange membrane fuel cells and electrolysers: a review *Int. J. Hydrog. Energy* **42** 28515–36
[34] Faustini M *et al* 2019 Hierarchically structured ultraporous iridium-based materials: a novel catalyst architecture for proton exchange membrane water electrolyzers *Adv. Energy Mater.* **9** 1802136
[35] Huang B, Xu H, Jiang N, Wang M, Huang J and Guan L 2022 Tensile-strained RuO_2 loaded on antimony-tin oxide by fast quenching for proton-exchange membrane water electrolyzer *Adv. Sci.* **9** 2201654
[36] Lv H, Wang S, Li J, Shao C, Zhou W, Shen X, Xue M and Zhang C 2020 Self-assembled RuO_2@IrO_x core-shell nanocomposite as high efficient anode catalyst for PEM water electrolyzer *Appl. Surf. Sci.* **514** 145943
[37] Kim H, Kim J, Kim S-K and Ahn S H 2018 A transition metal oxysulfide cathode for the proton exchange membrane water electrolyzer *Appl. Catal.* B **232** 93–100
[38] Schröder J, Mints V A, Bornet A, Berner E, Fathi Tovini M, Quinson J, Wiberg G K H, Bizzotto F, El-Sayed H A and Arenz M 2021 The gas diffusion electrode setup as straightforward testing device for proton exchange membrane water electrolyzer catalysts *JACS Au* **1** 247–51
[39] Mauger S A, Pfeilsticker J R, Wang M, Medina S, Yang-Neyerlin A C, Neyerlin K C, Stetson C, Pylypenko S and Ulsh M 2020 Fabrication of high-performance gas-diffusion-electrode based membrane-electrode assemblies *J. Power Sources* **450** 227581
[40] Breitwieser M, Klingele M, Vierrath S, Zengerle R and Thiele S 2018 Tailoring the membrane-electrode interface in PEM fuel cells: a review and perspective on novel engineering approaches *Adv. Energy Mater.* **8** 1701257
[41] Kang Z *et al* 2018 Novel thin/tunable gas diffusion electrodes with ultra-low catalyst loading for hydrogen evolution reactions in proton exchange membrane electrolyzer cells *Nano Energy* **47** 434–41
[42] Rabiee H, Ge L, Zhang X, Hu S, Li M and Yuan Z 2021 Gas diffusion electrodes (GDEs) for electrochemical reduction of carbon dioxide, carbon monoxide, and dinitrogen to value-added products: a review *Energy Environ. Sci.* **14** 1959–2008
[43] Nguyen T N and Dinh C-T 2020 Gas diffusion electrode design for electrochemical carbon dioxide reduction *Chem. Soc. Rev.* **49** 7488–504
[44] Talukdar K, Morawietz T, Sarkezi-Selsky P, Yezerska K, Sergeev O, Heger J-F, Jahnke T, Gazdzicki P and Friedrich K A 2022 Exploring critical parameters of electrode fabrication in polymer electrolyte membrane fuel cells *J. Power Sources* **540** 231638
[45] Mauger S A *et al* 2021 Development of high-performance roll-to-roll-coated gas-diffusion-electrode-based fuel cells *J. Power Sources* **506** 230039
[46] Thanasilp S and Hunsom M 2010 Effect of MEA fabrication techniques on the cell performance of Pt–Pd/C electrocatalyst for oxygen reduction in PEM fuel cell *Fuel* **89** 3847–52
[47] Gomes Bezerra C A, Deiner L J and Tremiliosi-Filho G 2019 Unexpected performance of inkjet-printed membrane electrode assemblies for proton exchange membrane fuel cells *Adv. Eng. Mater.* **21** 1900703
[48] Prasanna M, Ha H Y, Cho E A, Hong S-A and Oh I-H 2004 Investigation of oxygen gain in polymer electrolyte membrane fuel cells *J. Power Sources* **137** 1–8
[49] Moghaddam R B and Easton E B 2020 The interplay between impedance parameters, structure, and performance of fuel cell catalyst layers *Chem. Eng. Sci.* **224** 115792
[50] Bühler M, Holzapfel P, McLaughlin D and Thiele S 2019 From catalyst coated membranes to porous transport electrode based configurations in PEM water electrolyzers *J. Electrochem. Soc.* **166** F1070–F8
[51] Cho H J, Jang H, Lim S, Cho E, Lim T-H, Oh I-H, Kim H-J and Jang J H 2011 Development of a novel decal transfer process for fabrication of high-performance and reliable membrane electrode assemblies for PEMFCs *Int. J. Hydrog. Energy* **36** 12465–73
[52] Shahgaldi S, Alaefour I and Li X 2018 Impact of manufacturing processes on proton exchange membrane fuel cell performance *Appl. Energy* **225** 1022–32
[53] Akella S H, Ebenezer D, Sai Siddhardha R S, Ahire A and Mal N K 2018 Studies on structure property relations of efficient decal substrates for industrial grade membrane electrode assembly development in PEMFC *Sci. Rep.* **8** 12082
[54] Kyeong M, Chae J E, Lee S Y, Lim T-H, Kim M, Lee S-S, Song K H and Kim H-J 2022 Development of poly(arylene ether sulfone)-based blend membranes containing aliphatic moieties for the low-temperature decal transfer method *J. Membr. Sci.* **660** 120853
[55] Park J, Kang Z, Bender G, Ulsh M and Mauger S A 2020 Roll-to-roll production of catalyst coated membranes for low-temperature electrolyzers *J. Power Sources* **479** 228819
[56] Sung C-C, Liu C-Y and Cheng C C J 2014 Performance improvement by a glue-functioned Nafion layer coating on gas diffusion electrodes in PEM fuel cells *Int. J. Hydrog. Energy* **39** 11700–5
[57] Xing Y, Liu L, Li Z, Li Y, Fu Z and Li H 2022 Performance of an ePTFE-reinforced membrane electrode assembly for proton-exchange membrane fuel cells *Energy Fuels* **36** 11177–85
[58] Klingele M, Vierrath S, Breitwieser M, Klose C and Thiele S 2017 Direct membrane deposition—a fast and simple technique for membrane electrode assembly manufacturing *ECS Trans.* **80** 571–6
[59] Stähler M, Stähler A, Scheepers F, Carmo M and Stolten D 2019 A completely slot die coated membrane electrode assembly *Int. J. Hydrog. Energy* **44** 7053–8
[60] Holzapfel P, Bühler M, van Pham C, Hegge F, Böhm T, McLaughlin D, Breitwieser M and Thiele S 2020 Directly coated membrane electrode assemblies for proton exchange membrane water electrolysis *Electrochem. Commun.* **110** 106640
[61] Yang C, Han N, Wang Y, Yuan X-Z, Xu J, Huang H, Fan J, Li H and Wang H 2020 A novel approach to fabricate membrane electrode assembly by directly coating the Nafion ionomer on catalyst layers for proton-exchange membrane fuel cells *ACS Sustain. Chem. Eng.* **8** 9803–12
[62] Shang Z, Hossain M M, Wycisk R and Pintauro P N 2022 Poly(phenylene sulfonic acid)-expanded polytetrafluoroethylene composite membrane for low relative humidity operation in hydrogen fuel cells *J. Power Sources* **535** 231375
[63] Lim J, Park D, Jeon S S, Roh C-W, Choi J, Yoon D, Park M, Jung H and Lee H 2018 Ultrathin IrO_2 nanoneedles for electrochemical water oxidation *Adv. Funct. Mater.* **28** 1704796
[64] Xie Z *et al* 2021 Ultrathin platinum nanowire based electrodes for high-efficiency hydrogen generation in practical electrolyzer cells *Chem. Eng. J.* **410** 128333
[65] Kang Z, Chen Y, Wang H, Alia S M, Pivovar B S and Bender G 2022 Discovering and demonstrating a novel high-performing 2D-patterned electrode for proton-exchange membrane water electrolysis devices *ACS Appl. Mater. Interfaces* **14** 2335–42

[66] Liang S, Jiang M, Luo H, Ma Y and Yang J 2021 A high-rate electrode with Grotthuss topochemistry for membrane-free decoupled acid water electrolysis *Adv. Energy Mater.* **11** 2102057
[67] Ma Y, Guo Z, Dong X, Wang Y and Xia Y 2019 Organic proton-buffer electrode to separate hydrogen and oxygen evolution in acid water electrolysis *Angew. Chem., Int. Ed.* **58** 4622–6
[68] Wang J, Ji L, Teng X, Liu Y, Guo L and Chen Z 2019 Decoupling half-reactions of electrolytic water splitting by integrating a polyaniline electrode *J. Mater. Chem.* A **7** 13149–53
[69] Chen L, Dong X, Wang Y and Xia Y 2016 Separating hydrogen and oxygen evolution in alkaline water electrolysis using nickel hydroxide *Nat. Commun.* **7** 11741
[70] Ma Y, Dong X, Wang Y and Xia Y 2018 Decoupling hydrogen and oxygen production in acidic water electrolysis using a polytriphenylamine-based battery electrode *Angew. Chem., Int. Ed.* **57** 2904–8
[71] Landman A, Dotan H, Shter G E, Wullenkord M, Houaijia A, Maljusch A, Grader G S and Rothschild A 2017 Photoelectrochemical water splitting in separate oxygen and hydrogen cells *Nat. Mater.* **16** 646–51
[72] Peng X, Satjaritanun P, Taie Z, Wiles L, Keane A, Capuano C, Zenyuk I V and Danilovic N 2021 Insights into interfacial and bulk transport phenomena affecting proton exchange membrane water electrolyzer performance at ultra-low iridium loadings *Adv. Sci.* **8** 2102950
[73] Bühler M, Hegge F, Holzapfel P, Bierling M, Suermann M, Vierrath S and Thiele S 2019 Optimization of anodic porous transport electrodes for proton exchange membrane water electrolyzers *J. Mater. Chem.* A **7** 26984–95
[74] Stiber S *et al* 2021 Porous transport layers for proton exchange membrane electrolysis under extreme conditions of current density, temperature, and pressure *Adv. Energy Mater.* **11** 2100630
[75] Liu Y, Huang S, Wang D, Zhang H, Shan D, Peng S, Shen G, Wang L and Wang X 2022 Modifying Ti-based gas diffusion layer passivation for polymer electrolyte membrane water electrolysis via electrochemical nitridation *ACS Appl. Mater. Interfaces* **14** 15728–35
[76] Doan T L, Lee H E, Kim M, Cho W C, Cho H S and Kim T 2022 Influence of IrO_2/TiO_2 coated titanium porous transport layer on the performance of PEM water electrolysis *J. Power Sources* **533** 231370
[77] Bystron T, Vesely M, Paidar M, Papakonstantinou G, Sundmacher K, Bensmann B, Hanke-Rauschenbach R and Bouzek K 2018 Enhancing PEM water electrolysis efficiency by reducing the extent of Ti gas diffusion layer passivation *J. Appl. Electrochem.* **48** 713–23
[78] Lee B-S *et al* 2016 Polarization characteristics of a low catalyst loading PEM water electrolyzer operating at elevated temperature *J. Power Sources* **309** 127–34
[79] Stern M and Wissenberg H 1959 The influence of noble metal alloy additions on the electrochemical and corrosion behavior of titanium *J. Electrochem. Soc.* **106** 759
[80] Gago A S *et al* 2016 Protective coatings on stainless steel bipolar plates for proton exchange membrane (PEM) electrolysers *J. Power Sources* **307** 815–25
[81] Gabe D R 2014 *Principles of Metal Surface Treatment and Protection: Pergamon International Library of Science, Technology, Engineering and Social Studies: International Series on Materials Science and Technology* (Amsterdam: Elsevier)
[82] Liu C, Carmo M, Bender G, Everwand A, Lickert T, Young J L, Smolinka T, Stolten D and Lehnert W 2018 Performance enhancement of PEM electrolyzers through iridium-coated titanium porous transport layers *Electrochem. Commun.* **97** 96–99
[83] Feng M, Qu R, Wei Z, Wang L, Sun P and Wang Z 2015 Characterization of the thermolysis products of Nafion membrane: a potential source of perfluorinated compounds in the environment *Sci. Rep.* **5** 9859
[84] Schalenbach M, Carmo M, Fritz D L, Mergel J and Stolten D 2013 Pressurized PEM water electrolysis: efficiency and gas crossover *Int. J. Hydrog. Energy* **38** 14921–33
[85] Briguglio N, Siracusano S, Bonura G, Sebastián D and Aricò A S 2019 Flammability reduction in a pressurised water electrolyser based on a thin polymer electrolyte membrane through a Pt-alloy catalytic approach *Appl. Catal.* B **246** 254–65
[86] Yu T H, Sha Y, Liu W-G, Merinov B V, Shirvanian P and Goddard W A III 2011 Mechanism for degradation of Nafion in PEM fuel cells from quantum mechanics calculations *J. Am. Chem. Soc.* **133** 19857–63
[87] Papakonstantinou G, Algara-Siller G, Teschner D, Vidaković-Koch T, Schlögl R and Sundmacher K 2020 Degradation study of a proton exchange membrane water electrolyzer under dynamic operation conditions *Appl. Energy* **280** 115911
[88] Nguyen H, Lombeck F, Schwarz C, Heizmann P A, Adamski M, Lee H-F, Britton B, Holdcroft S, Vierrath S and Breitwieser M 2021 Hydrocarbon-based Pemion™ proton exchange membrane fuel cells with state-of-the-art performance *Sustain. Energy Fuels* **5** 3687–99
[89] Peighambardoust S J, Rowshanzamir S and Amjadi M 2010 Review of the proton exchange membranes for fuel cell applications *Int. J. Hydrog. Energy* **35** 9349–84
[90] Pianca M, Barchiesi E, Esposto G and Radice S 1999 End groups in fluoropolymers *J. Fluor. Chem.* **95** 71–84
[91] Klose C, Saatkamp T, Münchinger A, Bohn L, Titvinidze G, Breitwieser M, Kreuer K-D and Vierrath S 2020 All-hydrocarbon MEA for PEM water electrolysis combining low hydrogen crossover and high efficiency *Adv. Energy Mater.* **10** 1903995
[92] Park J E, Kim J, Han J, Kim K, Park S, Kim S, Park H S, Cho Y-H, Lee J-C and Sung Y-E 2021 High-performance proton-exchange membrane water electrolysis using a sulfonated poly(arylene ether sulfone) membrane and ionomer *J. Membr. Sci.* **620** 118871
[93] Jalani N H, Dunn K and Datta R 2005 Synthesis and characterization of Nafion®-MO_2 (M=Zr, Si, Ti) nanocomposite membranes for higher temperature PEM fuel cells *Electrochim. Acta* **51** 553–60
[94] Mishra A K, Bose S, Kuila T, Kim N H and Lee J H 2012 Silicate-based polymer-nanocomposite membranes for polymer electrolyte membrane fuel cells *Prog. Polym. Sci.* **37** 842–69
[95] Sugumar M and Dharmalingam S 2020 Statistical optimization of process parameters in microbial fuel cell for enhanced power production using sulphonated polyhedral oligomeric silsesquioxane dispersed sulphonated polystyrene ethylene butylene polystyrene nanocomposite membranes *J. Power Sources* **469** 228400
[96] Giancola S, Zatoń M, Reyes-Carmona Á, Dupont M, Donnadio A, Cavaliere S, Rozière J and Jones D J 2019 Composite short side chain PFSA membranes for PEM water electrolysis *J. Membr. Sci.* **570–1** 69–76
[97] Chee W K, Lim H N, Huang N M and Harrison I 2015 Nanocomposites of graphene/polymers: a review *RSC Adv.* **5** 68014–51
[98] Mahdi F, Naji L and Rahmanian A 2021 Fabrication of membrane electrode assembly based on Nafion/sulfonated graphene oxide nanocomposite by electroless deposition for proton exchange membrane fuel cells *Surf. Interfaces* **23** 100925
[99] Waribam P, Jaiyen K, Samart C, Ogawa M, Guan G and Kongparakul S 2022 MXene-copper oxide/sulfonated polyether ether ketone as a hybrid composite proton exchange membrane in electrochemical water electrolysis *Catal. Today* **407** 96–106
[100] Hong N V M, Huang H, Zhou K, Lee P S, Que W, Xu J Z and Kong L B 2017 Recent progress in layered transition metal carbides and/or nitrides (MXenes) and their composites: synthesis and applications *J. Mater. Chem.* A **5** 3039–68

[101] Lalia B S, Kochkodan V, Hashaikeh R and Hilal N 2013 A review on membrane fabrication: structure, properties and performance relationship *Desalination* **326** 77–95
[102] Siracusano S, Oldani C, Navarra M A, Tonella S, Mazzapioda L, Briguglio N and Aricò A S 2019 Chemically stabilised extruded and recast short side chain Aquivion® proton exchange membranes for high current density operation in water electrolysis *J. Membr. Sci.* **578** 136–48
[103] Bernt M, Siebel A and Gasteiger H A 2018 Analysis of voltage losses in PEM water electrolyzers with low platinum group metal loadings *J. Electrochem. Soc.* **165** F305–F14
[104] Ayers K E, Anderson E B, Capuano C, Carter B, Dalton L, Hanlon G, Manco J and Niedzwiecki M 2010 Research advances towards low cost, high efficiency PEM electrolysis *ECS Trans.* **33** 3
[105] Carmo M, Fritz D L, Mergel J and Stolten D 2013 A comprehensive review on PEM water electrolysis *Int. J. Hydrog. Energy* **38** 4901–34
[106] Tackett B M, Sheng W and Chen J G 2017 Opportunities and challenges in utilizing metal-modified transition metal carbides as low-cost electrocatalysts *Joule* **1** 253–63
[107] Minke C, Suermann M, Bensmann B and Hanke-Rauschenbach R 2021 Is iridium demand a potential bottleneck in the realization of large-scale PEM water electrolysis? *Int. J. Hydrog. Energy* **46** 23581–90
[108] Liu D *et al* 2019 Atomically dispersed platinum supported on curved carbon supports for efficient electrocatalytic hydrogen evolution *Nat. Energy* **4** 512–8
[109] Wee J-H, Lee K-Y and Kim S H 2007 Fabrication methods for low-Pt-loading electrocatalysts in proton exchange membrane fuel cell systems *J. Power Sources* **165** 667–77
[110] Li Z, Ge R, Su J and Chen L 2020 Recent progress in low Pt content electrocatalysts for hydrogen evolution reaction *Adv. Mater. Interfaces* **7** 2000396
[111] Wang Y, Yu X, Liu G, Zhu X, Xu R, Ji M, Ma Y and Ma L 2019 One-step fabrication of ultralow Pt loading high efficiency proton exchange membrane for water electrolysis by conventional E-beam metal deposition *Adv. Sustain. Syst.* **3** 1900026
[112] Shiva Kumar S and Himabindu V 2020 Boron-doped carbon nanoparticles supported palladium as an efficient hydrogen evolution electrode in PEM water electrolysis *Renew. Energy* **146** 2281–90
[113] Mo J, Stefanov B I, Lau T H M, Chen T, Wu S, Wang Z, Gong X-Q, Wilkinson I, Schmid G and Tsang S C E 2019 Superior performance of Ag over Pt for hydrogen evolution reaction in water electrolysis under high overpotentials *ACS Appl. Energy Mater.* **2** 1221–8
[114] Sun H, Yan Z, Liu F, Xu W, Cheng F and Chen J 2020 Self-supported transition-metal-based electrocatalysts for hydrogen and oxygen evolution *Adv. Mater.* **32** 1806326
[115] Hurd A J, Kelley R L, Eggert R G and Lee M-H 2012 Energy-critical elements for sustainable development *MRS Bull.* **37** 405–10
[116] Yuan C-Z *et al* 2021 Regulating intrinsic electronic structures of transition-metal-based catalysts and the potential applications for electrocatalytic water splitting *ACS Mater. Lett.* **3** 752–80
[117] Feng Q, Xiong Y, Xie L, Zhang Z, Lu X, Wang Y, Yuan X-Z, Fan J, Li H and Wang H 2019 Tungsten carbide encapsulated in grape-like N-doped carbon nanospheres: one-step facile synthesis for low-cost and highly active electrocatalysts in proton exchange membrane water electrolyzers *ACS Appl. Mater. Interfaces* **11** 25123–32
[118] Morozan A, Johnson H, Roiron C, Genay G, Aldakov D, Ghedjatti A, Nguyen C T, Tran P D, Kinge S and Artero V 2020 Nonprecious bimetallic iron–molybdenum sulfide electrocatalysts for the hydrogen evolution reaction in proton Exchange membrane electrolyzers *ACS Catal.* **10** 14336–48
[119] Mo J, Wu S, Lau T H M, Kato R, Suenaga K, Wu T-S, Soo Y-L, Foord J S and Tsang S C E 2020 Transition metal atom–doped monolayer MoS_2 in a proton-exchange membrane electrolyzer *Mater. Today Adv.* **6** 100020
[120] Kim J H, Kim H, Kim J, Lee H J, Jang J H and Ahn S H 2018 Electrodeposited molybdenum sulfide as a cathode for proton exchange membrane water electrolyzer *J. Power Sources* **392** 69–78
[121] Hinnemann B, Moses P G, Bonde J, Jørgensen K P, Nielsen J H, Horch S, Chorkendorff I and Nørskov J K 2005 Biomimetic hydrogen evolution: MoS_2 nanoparticles as catalyst for hydrogen evolution *J. Am. Chem. Soc.* **127** 5308–9
[122] Jaramillo T F, Jørgensen K P, Bonde J, Nielsen J H, Horch S and Chorkendorff I 2007 Identification of active edge sites for electrochemical H_2 evolution from MoS_2 nanocatalysts *Science* **317** 100–2
[123] Holzapfel P K R, Bühler M, Escalera-López D, Bierling M, Speck F D, Mayrhofer K J J, Cherevko S, Pham C V and Thiele S 2020 Fabrication of a robust PEM water electrolyzer based on non-noble metal cathode catalyst: $[Mo3S13]^{2-}$ clusters anchored to N-doped carbon nanotubes *Small* **16** 2003161
[124] Lee W H, Ko Y-J, Kim J H, Choi C H, Chae K H, Kim H, Hwang Y J, Min B K, Strasser P and Oh H-S 2021 High crystallinity design of Ir-based catalysts drives catalytic reversibility for water electrolysis and fuel cells *Nat. Commun.* **12** 4271
[125] Hussain S, Erikson H, Kongi N, Sarapuu A, Solla-Gullón J, Maia G, Kannan A M, Alonso-Vante N and Tammeveski K 2020 Oxygen reduction reaction on nanostructured Pt-based electrocatalysts: a review *Int. J. Hydrog. Energy* **45** 31775–97
[126] Choi K J, Kim H and Kim S-K 2021 Multicomponent nonprecious hydrogen evolution catalysts for high performance and durable proton exchange membrane water electrolyzer *J. Power Sources* **506** 230200
[127] Kim J H, Kim J, Kim H, Kim J and Ahn S H 2019 Facile fabrication of nanostructured NiMo cathode for high-performance proton exchange membrane water electrolyzer *J. Ind. Eng. Chem.* **79** 255–60
[128] Yoon Y, Kim H, Kim S-K and Kim J J 2021 Acid-durable, high-performance cobalt phosphide catalysts for hydrogen evolution in proton exchange membrane water electrolysis *Int. J. Energy Res.* **45** 16842–55
[129] Wei Z, Guo M and Zhang Q 2023 Scalable electrodeposition of NiFe-based electrocatalysts with self-evolving multi-vacancies for high-performance industrial water electrolysis *Appl. Catal.* B **322** 122101
[130] Bellini M, Bevilacqua M, Marchionni A, Miller H A, Filippi J, Grützmacher H and Vizza F 2018 Energy production and storage promoted by organometallic complexes *Eur. J. Inorg. Chem.* **2018** 4393–412
[131] Bellini M *et al* 2022 Remarkable stability of a molecular ruthenium complex in PEM water electrolysis *Chem. Sci.* **13** 3748–60
[132] Ogawa T, Takeuchi M and Kajikawa Y 2018 Analysis of trends and emerging technologies in water electrolysis research based on a computational method: a comparison with fuel cell research *Sustainability* **10** 478
[133] Taniguchi A, Akita T, Yasuda K and Miyazaki Y 2004 Analysis of electrocatalyst degradation in PEMFC caused by cell reversal during fuel starvation *J. Power Sources* **130** 42–49
[134] Lim K H, Lee W H, Jeong Y and Kim H 2017 Analysis of carbon corrosion in anode under fuel starvation using on-line mass spectrometry in polymer electrolyte membrane fuel cells *J. Electrochem. Soc.* **164** F1580
[135] Kim J, Kim J, Kim H and Ahn S H 2019 Nanoporous nickel phosphide cathode for a high-performance proton exchange membrane water electrolyzer *ACS Appl. Mater. Interfaces* **11** 30774–85

[136] Xue X, Zhang M, Wei F, Liang C, Liang J, Li J, Cheng W, Deng K and Liu W 2022 Gold as an efficient hydrogen isotope separation catalyst in proton exchange membrane water electrolysis *Int. J. Hydrog. Energy* **47** 26842–9
[137] Zhang W and Zhou K 2017 Ultrathin two-dimensional nanostructured materials for highly efficient water oxidation *Small* **13** 1700806
[138] Sugawara Y, Hihara T, Anilkumar G M, Kamata K and Yamaguchi T 2021 Metal oxide electrocatalyst support for carbon-free durable electrodes with excellent corrosion resistance at high potential conditions *Sustain. Energy Fuels* **5** 1374–8
[139] Lebedev D *et al* 2017 Highly active and stable iridium pyrochlores for oxygen evolution reaction *Chem. Mater.* **29** 5182–91
[140] Oakton E, Lebedev D, Povia M, Abbott D F, Fabbri E, Fedorov A, Nachtegaal M, Copéret C and Schmidt T J 2017 IrO_2-TiO_2: a high-surface-area, active, and stable electrocatalyst for the oxygen evolution reaction *ACS Catal.* **7** 2346–52
[141] Siracusano S, Baglio V, D'Urso C, Antonucci V and Aricò A S 2009 Preparation and characterization of titanium suboxides as conductive supports of IrO_2 electrocatalysts for application in SPE electrolysers *Electrochim. Acta* **54** 6292–9
[142] Regmi Y N, Tzanetopoulos E, Zeng G, Peng X, Kushner D I, Kistler T A, King L A and Danilovic N 2020 Supported oxygen evolution catalysts by design: toward lower precious metal loading and improved conductivity in proton exchange membrane water electrolyzers *ACS Catal.* **10** 13125–35
[143] Min X *et al* 2021 High performance and cost-effective supported IrO_x catalyst for proton exchange membrane water electrolysis *Electrochim. Acta* **385** 138391
[144] Lv H, Wang S, Hao C, Zhou W, Li J, Xue M and Zhang C 2019 Oxygen-deficient $Ti_{0.9}Nb_{0.1}O_{2-x}$ as an efficient anodic catalyst support for PEM water electrolyzer *Chem.Cat.Chem.* **11** 2511–9
[145] Lin X, Ng S-F and Ong W-J 2022 Coordinating single-atom catalysts on two-dimensional nanomaterials: a paradigm towards bolstered photocatalytic energy conversion *Coord. Chem. Rev.* **471** 214743
[146] Chia X and Pumera M 2018 Characteristics and performance of two-dimensional materials for electrocatalysis *Nat. Catal.* **1** 909–21
[147] Chen J *et al* 2019 Low-coordinate iridium oxide confined on graphitic carbon nitride for highly efficient oxygen evolution *Angew. Chem., Int. Ed.* **58** 12540–4
[148] Gong Y, Li M, Li H and Wang Y 2015 Graphitic carbon nitride polymers: promising catalysts or catalyst supports for heterogeneous oxidation and hydrogenation *Green Chem.* **17** 715–36
[149] Wang S, Lv H, Tang F, Sun Y, Ji W, Zhou W, Shen X and Zhang C 2021 Defect engineering assisted support effect: IrO_2/N defective g-C_3N_4 composite as highly efficient anode catalyst in PEM water electrolysis *Chem. Eng. J.* **419** 129455
[150] Lim J, Kang G, Lee J W, Jeon S S, Jeon H, Kang P W and Lee H 2022 Amorphous Ir atomic clusters anchored on crystalline IrO_2 nanoneedles for proton exchange membrane water oxidation *J. Power Sources* **524** 231069
[151] Li X and Wang J 2020 One-dimensional and two-dimensional synergized nanostructures for high-performing energy storage and conversion *InfoMat* **2** 3–32
[152] Jiang G, Yu H, Li Y, Yao D, Chi J, Sun S and Shao Z 2021 Low-loading and highly stable membrane electrode based on an Ir@WO_xNR ordered array for PEM water electrolysis *ACS Appl. Mater. Interfaces* **13** 15073–82
[153] Hegge F, Lombeck F, Cruz Ortiz E, Bohn L, von Holst M, Kroschel M, Hübner J, Breitwieser M, Strasser P and Vierrath S 2020 Efficient and stable low iridium loaded anodes for PEM water electrolysis made possible by nanofiber interlayers *ACS Appl. Energy Mater.* **3** 8276–84
[154] Hrbek T, Kúš P, Yakovlev Y, Nováková J, Lobko Y, Khalakhan I, Matolín V and Matolínová I 2020 Sputter-etching treatment of proton-exchange membranes: completely dry thin-film approach to low-loading catalyst-coated membranes for water electrolysis *Int. J. Hydrog. Energy* **45** 20776–86
[155] Kim H, Kim J, Kim J, Han G H, Guo W, Hong S, Park H S, Jang H W, Kim S Y and Ahn S H 2021 Dendritic gold-supported iridium/iridium oxide ultra-low loading electrodes for high-performance proton exchange membrane water electrolyzer *Appl. Catal.* B **283** 119596
[156] Cha J I, Baik C, Lee S W and Pak C 2022 Improved utilization of IrO_x on Ti_4O_7 supports in membrane electrode assembly for polymer electrolyte membrane water electrolyzer *Catal. Today* **403** 19–27
[157] Saveleva V A *et al* 2020 Insight into the mechanisms of high activity and stability of iridium supported on antimony-doped tin oxide aerogel for anodes of proton exchange membrane water electrolyzers *ACS Catal.* **10** 2508–16
[158] Li Y, Sun Y, Qin Y, Zhang W, Wang L, Luo M, Yang H and Guo S 2020 Recent advances on water-splitting electrocatalysis mediated by noble-metal-based nanostructured materials *Adv. Energy Mater.* **10** 1903120
[159] Bhowmik T, Kundu M K and Barman S 2016 Growth of one-dimensional RuO_2 nanowires on g-carbon nitride: an active and stable bifunctional electrocatalyst for hydrogen and oxygen evolution reactions at all pH values *ACS Appl. Mater. Interfaces* **8** 28678–88
[160] Zhang F, Sherrell P C, Luo W, Chen J, Li W, Yang J and Zhu M 2021 Organic/inorganic hybrid fibers: controllable architectures for electrochemical energy applications *Adv. Sci.* **8** 2102859
[161] Shiva Kumar S, Ramakrishna S U B, Bhagawan D and Himabindu V 2018 Preparation of $Ru_xPd_{1-x}O_2$ electrocatalysts for the oxygen evolution reaction (OER) in PEM water electrolysis *Ionics* **24** 2411–9
[162] Kaya M F, Demir N, Rees N V and El-Kharouf A 2021 Magnetically modified electrocatalysts for oxygen evolution reaction in proton exchange membrane (PEM) water electrolyzers *Int. J. Hydrog. Energy* **46** 20825–34
[163] Fan Z, Yu H, Jiang G, Yao D, Sun S, Chi J, Qin B and Shao Z 2022 Low precious metal loading porous transport layer coating and anode catalyst layer for proton exchange membrane water electrolysis *Int. J. Hydrog. Energy* **47** 18963–71
[164] Joo J, Kim T, Lee J, Choi S-I and Lee K 2019 Morphology-controlled metal sulfides and phosphides for electrochemical water splitting *Adv. Mater.* **31** 1806682
[165] Park J E *et al* 2019 Ultra-low loading of IrO_2 with an inverse-opal structure in a polymer-exchange membrane water electrolysis *Nano Energy* **58** 158–66
[166] He D, Zhang C, Zeng G, Yang Y, Huang D, Wang L and Wang H 2019 A multifunctional platform by controlling of carbon nitride in the core-shell structure: from design to construction, and catalysis applications *Appl. Catal.* B **258** 117957
[167] Gao J, Liu Y, Liu B and Huang K-W 2022 Progress of heterogeneous iridium-based water oxidation catalysts *ACS Nano* **16** 17761–77
[168] Zheng Y, Zhang F, Wang G, Lai D, Zou L, Cheng Q, Li J, Zou Z and Yang H 2022 CO induced phase-segregation to construct robust and efficient $IrRu_x$@Ir core-shell electrocatalyst towards acidic oxygen evolution *J. Power Sources* **528** 231189
[169] Pham C V, Bühler M, Knöppel J, Bierling M, Seeberger D, Escalera-López D, Mayrhofer K J J, Cherevko S and Thiele S 2020 IrO_2 coated TiO_2 core-shell microparticles advance performance of low loading proton exchange membrane water electrolyzers *Appl. Catal.* B **269** 118762

[170] Möckl M, Ernst M F, Kornherr M, Allebrod F, Bernt M, Byrknes J, Eickes C, Gebauer C, Moskovtseva A and Gasteiger H A 2022 Durability testing of low-iridium PEM water electrolysis membrane electrode assemblies *J. Electrochem. Soc.* **169** 064505
[171] Pantò F, Siracusano S, Briguglio N and Aricò A S 2020 Durability of a recombination catalyst-based membrane-electrode assembly for electrolysis operation at high current density *Appl. Energy* **279** 115809
[172] Burnett D L, Petrucco E, Rigg K M, Zalitis C M, Lok J G, Kashtiban R J, Lees M R, Sharman J D B and Walton R I 2020 (M,Ru)O_2 (M = Mg, Zn, Cu, Ni, Co) rutiles and their use as oxygen evolution electrocatalysts in membrane electrode assemblies under acidic conditions *Chem. Mater.* **32** 6150–60
[173] Anastas P T and Zimmerman J B 2019 The periodic table of the elements of green and sustainable chemistry *Green Chem.* **21** 6545–66
[174] Dunn P J 2012 The importance of green chemistry in process research and development *Chem. Soc. Rev.* **41** 1452–61
[175] Mohamed A, Ibrahem H and Kim K 2022 Machine learning-based simulation for proton exchange membrane electrolyzer cell *Energy Rep.* **8** 13425–37
[176] Santaniello T and Milani P 2020 *Frontiers of Nanoscience* ed P Milani and M Sowwan (Amsterdam: Elsevier) pp 313–33
[177] Yuk H, Lu B, Lin S, Qu K, Xu J, Luo J and Zhao X 2020 3D printing of conducting polymers *Nat. Commun.* **11** 1604
[178] Bui J C, Davis J T and Esposito D V 2020 3D-printed electrodes for membraneless water electrolysis *Sustain. Energy Fuels* **4** 213–25
[179] Yang G, Yu S, Kang Z, Dohrmann Y, Bender G, Pivovar B S, Green J B, Retterer S T, Cullen D A and Zhang F-Y 2019 A novel PEMEC with 3D printed non-conductive bipolar plate for low-cost hydrogen production from water electrolysis *Energy Convers. Manage.* **182** 108–16
[180] Bogdan E and Michorczyk P 2020 3D printing in heterogeneous catalysis—the state of the art *Materials* **13** 4534
[181] Parra-Cabrera C, Achille C, Kuhn S and Ameloot R 2018 3D printing in chemical engineering and catalytic technology: structured catalysts, mixers and reactors *Chem. Soc. Rev.* **47** 209–30